Femtosecond Spectroscopic Study of Relaxation Processes of Three Amino-Substituted Coumarin Dyes in Methanol and Dimethyl Sulfoxide

T. Gustavsson,* L. Cassara, V. Gulbinas,† G. Gurzadyan,‡ J.-C. Mialocq, S. Pommeret, M. Sorgius, and P. van der Meulen§

CEA/Saclay, DSM/DRECAM/SCM, URA331 CNRS, F-91191, Gif-sur-Yvette, Cedex, France

Received: November 20, 1997; In Final Form: January 22, 1998

Time-resolved fluorescence spectra of three amino-substituted coumarin dyes have been recorded in methanol and dimethyl sulfoxide using the fluorescence upconversion technique with an apparatus response function of ≈200 fs fwhm. The three fluorinated coumarins are the 7-amino-4-trifluoromethylcoumarin (C151), the 7-diethylamino-4-trifluoromethylcoumarin (C35), and the rigidified aminocoumarin with a julolidine structure (C153). The dynamic Stokes shifts are found to be dominated by an ultrafast component with a characteristic time shorter than the present time resolution of ≈50 fs. The dynamic Stokes shifts are compared to estimations based on a "Kamlet and Taft" analysis of steady-state data in 20 solvents. It is found that the ultrafast component can be assigned mainly to intramolecular relaxation. The influences of photoinduced changes of solute−solvent hydrogen bonds on the observed spectral shifts are discussed. The breaking of hydrogen bonds at the amino group is very fast in both solvents and embedded in the ultrafast solvent inertial relaxation, while the reformation of hydrogen bonds at the carbonyl group is believed to occur on the 10−20 ps time scale in the hydrogen bond donating (HBD) solvent methanol. However, it is impossible to unambiguously correlate a particular experimental time constant with the breaking or the formation of a hydrogen bond.

I. Introduction

The 7-aminocoumarins constitute an important group of laser dyes in the blue-green spectral region.[1,2] It is well-known that the first excited singlet state S_1 of these molecules has a high dipole moment resulting from the electron donor nature of the amino group and the electron acceptor nature of the carbonyl group (see Scheme 1). The S_1 charge-transfer character grows with increasing the alkylation degree of the amino group, resulting in a strengthened stabilization of the excited state.[1−3] The high dipole moment of the S_1 state leads to very large Stokes shifts, strongly dependent on the solvent polarity, making the 7-aminocoumarins popular probe molecules in time-dependent fluorescence Stokes shift (TDFSS) measurements.[4−23]

Such studies have, with increasing time-resolution, gradually led to the establishment of the presence of an extremely rapid component (<100 fs), accounting for up to 50% of the spectral relaxation and assigned to inertial motion of the solvent molecules.[15,24,25] In particular, the rigid coumarin 153, considered to possess no intramolecular relaxation processes other than ultrafast vibrational relaxation, has been used in many of the above-mentioned TDFSS studies and most notably in two recent "state-of-the-art" works on solvation dynamics by Maroncelli and co-workers,[21,22] using fluorescence upconversion with 70 fs laser pulses.

Such an assumption may very well be true for a conformationally rigid molecule, but it cannot be assumed "ad hoc" for other coumarins with flexible amino groups which allow for internal dynamics. Indeed, 7-aminocoumarins display a rather complicated solvatochromism and the solvent-dependency of parameters such as the fluorescence quantum yield and lifetime are far from well understood. A fluorescence quenching (i.e., a nonradiative decay of the first excited S_1 singlet state) affects nearly all coumarin molecules, but in various ways. This quenching depends on the substituents, on the electron donor character, and/or the mobility of the amino group. It is nearly

SCHEME 1: 7-Aminocoumarins C151, C35, and C153

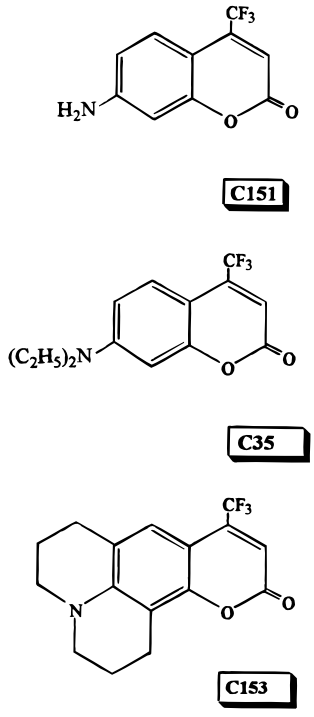

† Permanent address: Institute of Physics, A. Gaustato 12, 2600 Vilnius, Lithuania.

‡ Permanent address: National Academy of Sciences of Armenia, Yerevan, Armenia.

§ Present address: Dept. Physics I, KTH, Royal Institute of Technology, S-10044 Stockholm, Sweden.

S1089-5639(98)00282-5 CCC: $15.00
Published on Web 04/04/1998

nonexistent for the blocked coumarins but also for the unsubstituted aminocoumarins such as C120 as well. Different explanations based on intramolecular amino group dynamics have thus been put forward to explain this quenching process. A rotatory decay mechanism leading to a nonfluorescent twisted internal charge transfer (TICT) state has been proposed,[26−28] as well as a $sp^2 \rightarrow sp^3$ configurational change, the so-called umbrella-like motion (ULM), in the excited S_1 state.[3] The importance of specific solute−solvent interactions (i.e., hydrogen bonding has been put forward by several authors).[29,30] It was recently proposed that a pyramidalization of the amino group only constitutes the first step of the rotatory decay.[31]

Even for the "rigid" coumarin C153, the assumed absence of intramolecular relaxation processes has recently been contested. Using ultrafast (<40 fs) pump−probe spectroscopy, Kovalenko et al.[32] studied C153 in acetonitrile and methanol, and found indications for intramolecular electronic relaxation, although exciting in the red wing of the S_1-S_0 band. These conclusions were said to be in accordance with the earlier findings of Blanchard and co-workers, who, combining results from picosecond pump−probe spectroscopy and quantum chemistry calculations, proposed a multiple electronic state scheme in order to explain the S_1 state relaxation dynamics observed for C153 on the picosecond time scale.[33,34]

Very few time-resolved studies have directly addressed the solute influence on observed spectral relaxation dynamics. Jarzeba et al. investigated the solvation dynamics of the two coumarins C152 and C153 in various solvents using fluorescence upconversion.[13] They found the solvation of the 7-(dimethylamino)-4-trifluoromethylcoumarin (C152) to be 20−40% faster than for the blocked C153. Chapman et al. studied the solute dependence of solvation dynamics in 1-propanol at 253 K using time-correlated single-photon counting.[20] They considered, in particular, the ability of the solute molecule to form hydrogen bonds with the solvent. Among the various probe molecules they used, five different coumarins can be found, differing in alkyl substituents at position 7. They found that specific solute−solvent hydrogen bonding does not contribute to any significant degree to the observed solvation for the majority of the solutes, and least so for the coumarins. This is surprising in view of the fact that the influence of hydrogen bonding on steady-state spectral shifts is rather well established.[3,29,30]

The aim of the present work is to investigate the dynamic Stokes shifts of three different 7-aminocoumarins, C151, C35, and C153, see Scheme 1, with different properties with regards to internal degrees of freedom, charge-transfer character, and hydrogen bond formation with the surrounding solvent, in two polar solvents—methanol and dimethyl sulfoxide (DMSO)—with different hydrogen bonding character. Thus, the relaxation dynamics of the blocked C153 may be compared with those of C151 and C35, for which structural rearrangements of the amino group (i.e., *intra*molecular relaxation) are possible. Moreover, the influence of hydrogen bond dynamics (i.e., *inter*molecular relaxation) can be tested by comparing the dynamics of various combinations of protic/aprotic coumarins/solvents. To be more precise, C35 and C153 are acceptors of hydrogen bonds, while C151 is acceptor and donor. Methanol is donor and acceptor of hydrogen bonds, while DMSO is only acceptor.

To simplify the following discussion, the possible hydrogen bonds involved in the ground and the excited states of C35 and C151 are shown in Figure 1 (we use the same notation for the hydrogen bonds as Arbeloa et al.[3]). While both coumarins C35 and C151 may accept hydrogen bonds at the nitrogen lone pair

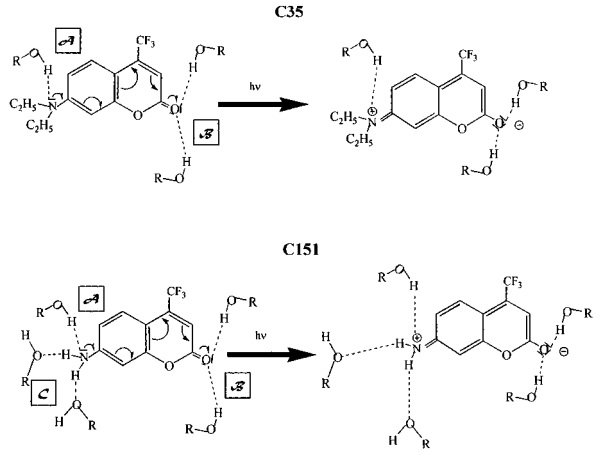

Figure 1. Simplified view of the possible hydrogen bonds involved in the ground and the excited states of C35 and C151. Hydrogen bonds may be formed on the nitrogen lone pair (type A) and the carbonyl group (type B) from hydrogen bond donating solvents, and on the two hydrogen atoms on the amino group (type C) from hydrogen bond accepting solvents. (The notation used for the hydrogen bonds is the same as that of Arbeloa et al.[3]). After photoexcitation, hydrogen bonds A and C are weakened while hydrogen bond B is strengthened.

(type A) and the carbonyl group (type B) from hydrogen bond donating solvents, only C151 may establish such bonds with hydrogen bond accepting solvents from the two H-atoms on the amino group (type C). The formation of solute−solvent exciplexes has even been put forward in the case of C151.[35]

II. Experimental Section

A. Chemicals and Steady-State Spectroscopy. 7-amino-4-trifluoromethylcoumarin (C151) and 7-diethylamino-4-trifluoromethyl-coumarin (C35) were purchased from Sigma Chemicals (both commercial grade) and the rigidified aminocoumarin with a julolidine structure (C153) from Lambda Physik (Lambdachrome laser dye). Methanol, ethanol, dimethylformamide (DMF), acetonitrile, tetrahydrofuran (THF), and *n*-hexane (Merck Uvasol, for spectroscopy); 1-propanol, *tert*-butyl alcohol, and ethyleneglycol (EG) (Merck, for analysis); 1-butanol, ethyl acetate (Merck, for chromatography); and dimethylacetamide (DMA) (Merck, for synthesis), dimethyl sulfoxide (DMSO), acetone, and formamide (Aldrich, spectrophotometric grade); 2-propanol (Prolabo, RECTAPUR) and diethyl ether ("Solvants Documentation Synthèses", for pure synthesis) were used without any further purification. Ultrapure water was obtained from a Waters MilliPore system. Solutions were prepared to have an optical density of about 0.5 at 394 nm for an optical path length of 1 mm corresponding to coumarin concentrations of about 5×10^{-4} mol dm^{-3}.

Steady-state absorption and emission spectra of the three coumarins in the above-mentioned solvents were recorded with a CARY 3E UV−visible absorption spectrophotometer and a SPEX Fluorolog 2F111A1 spectrofluorometer, respectively.

B. Femtosecond Emission Spectrometer−Instrumental Setup. Time-resolved emission spectra were obtained using the sum-frequency generation technique (also known as the "fluorescence upconversion" technique).[36−38] The setup used for this type of measurements has already been described.[39] A simplified overview of the setup is shown in Figure 2. We give here only a brief description in order to draw the attention to some particular features allowing the direct recording of time-resolved fluorescence spectra.

The femtosecond laser source was a Ti:sapphire laser (Coherent MIRA 900) pumped by a continuous wave Ar^+ laser

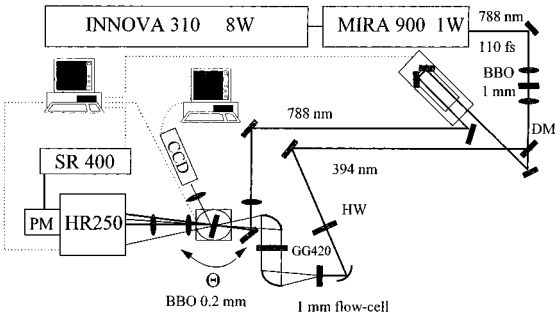

Figure 2. Schematic view of the experimental setup for the femtosecond fluorescence upconversion spectrometer. DM = dichroic mirror used to separate the second harmonic (394 nm) from the fundamental (788 nm). HW = half-wave plate used to control the polarization of the excitation pulse. GG420 is a Schott high-pass filter (in λ) used to eliminate scattered SHG light. PM = photomultiplier tube. CCD = video camera equipped with a charge-coupled device.

(Coherent INNOVA 310, 8W output power all lines). Typical performances of the Ti:sapphire laser were 1.2 W average output power (running in the mode-locked regime) at 788 nm and 76 MHz repetition rate. The second harmonic (SH) was generated in a 1 mm thick Type I BBO crystal (Fujian Institute) and separated from the residual fundamental light by a dichroic beam splitter. After passage through a delay line (Microcontrole UT100,125PP controlled by a ITL09 unit), the residual fundamental was focused by a 100 mm lens into a 0.2 mm Type II BBO crystal (Fujian Institute), thus serving as the gating pulse for the sum-frequency generation. The SH was used as excitation beam and was focused by a 1.5 in. off-axis parabolic mirror (Ealing 1.5 in. effective focal length at 60°) into the sample which was contained in a 1 mm thick flowing quartz cell (Ets Thuet-Biechelin). The fluorescence was collected by a 4 in. off-axis parabolic mirror (Ealing 4 in. effective focal length at 90°), passed through a 1 mm optical filter (Schott GG420), and was focused into the upconversion crystal by a 4 in. parabolic mirror, identical to the first one. The upconverted light (at about 300 nm) was collected by a 150 mm lens, passed through a 1 mm optical filter (Schott UG11), and was focused onto the entrance slit of a 0.25 m monochromator (Jobin Yvon, Instruments SA HR250) equipped with a 600 grooves/mm grating blazed at 350 nm. The slit width was kept at 0.5 mm, which corresponds to about 10 nm bandwidth. The spectrally selected upconversion light was detected by a photomultiplier (Hamamatsu R1527P) positioned after the monochromator and connected to a lock-in photon counter (Stanford SR400). All experiments were performed at magic angle between the polarization axes of excitation and observation.

The autocorrelation-trace of the Ti:sapphire laser output was obtained with a MC2 Femtoscope giving 195 fs full width at half-maximum (fwhm), best described by a sech^2 pulse with approximately 125 fs fwhm. The crosscorrelation trace between the laser fundamental (788 nm) and the second harmonic (394 nm) gives a fwhm value of 210 fs for the apparatus function. This was separately confirmed by recording the Raman lines of pure MeOH with the fluorescence upconversion setup, see Figure 3. In this figure one sees clearly the two strongest Raman lines of CH (υ_{Raman} = 2900 cm^{-1}) and OH (υ_{Raman} = 3500 cm^{-1}).[40] A temporal analysis, best described by a Gaussian line shape, gives a fwhm half width equal to 220 fs. We judge the experimental time-resolution to be ≈50 fs.

C. Data Acquisition and Automatization. The prevailing method to obtain time-resolved emission spectra when using the upconversion technique is the indirect spectral reconstruction

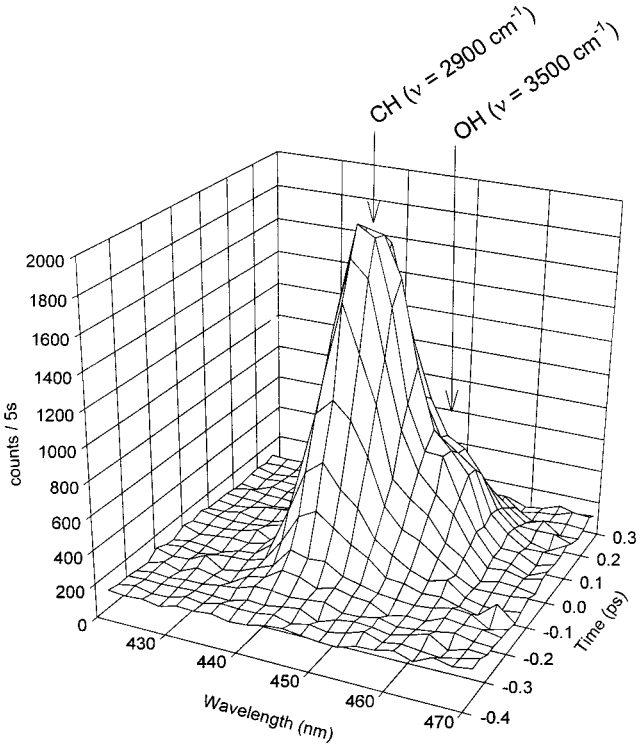

Figure 3. A 3D view of the Raman line of pure MeOH induced by the 394 nm excitation pulse and detected with the upconversion setup. One sees clearly the two strongest Raman lines of CH (υ_{Raman} 2900 cm^{-1}) and OH (υ_{Raman} = 3500 cm^{-1}). The temporal form is best described by a Gaussian shape with 220 fs half-width (fwhm).

method (SRM), originally developed by Maroncelli and Fleming.[4] We have proposed an alternative method,[39,41] which consists of the direct recording of time-resolved spectra instead of reconstructing them from kinetics. There are two points to keep in mind regarding this method. The first point is the fact that different spectral components of the fluorescence spectrum propagate with different velocities due to the group velocity difference (GVD) introduced by the refractive material present between the sample cell and the upconversion crystal. The second point to keep in mind is the limited bandwidth of the crystal.[36] In our case, with a thickness of 0.2 mm of the BBO crystal, the half bandwidth of sum frequency generation centered at 450 nm is only about 20 nm, which is much less than the typical 200 nm width of the fluorescence spectrum.

We have accounted for these two effects in our present experimental setup. While scanning the monochromator, the GVD is calculated as a function of wavelength and the difference in propagation time compensated for by adjusting the delay line. Likewise, the optimal phase matching angle is calculated as a function of wavelength and the crystal is rotated to the correct angular position. This is controlled by a master data acquisition program written in Visual Basic 3.0 and running under Windows 3.11. Typical integration times of the upconversion signal per data point were 2−3 s, giving about 1000 counts at the fluorescence maximum.

III. Steady-State Spectra: Results and Analysis

A. Absorption and Fluorescence Spectra. As described above, steady-state absorption and emission spectra of the three coumarins were recorded in 18 solvents of different polarity and hydrogen bonding character. The purpose was to acquire a large database, covering a broad spectrum of macroscopic solvent properties and lending itself to an unambiguous analysis

TABLE 1: Measured Mean Frequencies of the Absorption and Fluorescence Spectra, Observed Stokes Shifts $\Delta\nu$(obs), and Half-Widths of the Absorption and Fluorescence Spectra of Coumarins C151, C35, and C153 in Various Solvents. All Frequencies in Units of 10^3 cm^{-1}

solvent	ν (absorption)	ν (fluorescence)	$\Delta\nu$ (obs)	fwhm (abs)	fwhm (fluo)	solvent	ν (absorption)	ν (fluorescence)	$\Delta\nu$ (obs)	fwhm (abs)	fwhm (fluo)
					(a) C151						
n-hexane	29.84	23.64	6.19	4.26	4.13	DMF	27.04	19.97	7.06	4.42	3.64
diethyl ether	28.14	21.44	6.73	4.30	3.78	DMA	26.88	19.97	6.92	4.39	3.62
THF	27.72	21.01	6.70	4.35	3.68	methanol	27.35	19.62	7.73	4.66	3.56
1,4-dioxane	28.55	20.84	7.71	4.48	3.80	ethanol	27.03	19.80	7.23	4.56	3.52
ethyl acetate	28.12	21.27	6.84	4.42	3.70	2-propanol	26.80	19.92	6.88	4.54	3.47
acetone	27.48	20.63	6.85	4.46	3.68	1-butanol	26.86	19.85	7.01	4.54	3.47
acetonitrile	28.08	20.51	7.56	4.58	3.68	*tert*-butanol	26.83	20.05	6.78	4.54	3.45
DMSO	26.75	19.67	7.08	4.44	3.61	EG	27.08	19.29	7.78	4.75	3.54
formamide	27.24	19.46	7.79	4.77	3.55	water	28.06	19.13	8.93	5.53	3.58
					(b) C35						
n-hexane	27.22	22.79	4.42	3.64	3.79	DMF	25.47	18.77	6.70	4.05	3.62
diethyl ether	26.39	20.68	5.71	3.83	3.60	DMA	25.48	18.88	6.61	4.09	3.56
THF	26.02	19.91	6.11	3.96	3.55	methanol	25.48	18.36	7.12	4.07	3.60
1,4-dioxane	26.43	19.94	6.49	3.96	3.62	ethanol	25.10	18.67	6.44	4.19	3.60
ethyl acetate	26.18	20.00	6.18	3.98	3.56	1-propanol	25.57	18.86	6.71	4.03	3.54
acetone	25.86	19.30	6.56	4.06	3.58	2-propanol	25.66	19.01	6.65	4.05	3.54
acetonitrile	25.76	18.96	6.80	4.04	3.37	1-butanol	25.60	18.90	6.69	4.04	3.54
DMSO	25.27	18.39	6.88	4.09	3.34	*tert*-butanol	25.80	19.39	6.41	3.95	3.52
formamide	24.96	18.14	6.81	4.03	3.57	EG	25.58	18.10	7.48	4.08	3.58
					(c) C153						
n-hexane	26.26	21.60	4.66	3.66	3.41	DMF	24.33	17.93	6.39	4.07	3.41
diethyl ether	25.40	20.13	5.27	3.78	3.40	DMA	24.34	18.06	6.28	4.05	3.41
THF	25.08	19.07	6.01	4.21	3.45	methanol	24.35	17.58	6.77	4.16	3.38
1,4-dioxane	25.36	18.94	6.42	4.00	3.52	ethanol	24.39	17.83	6.56	4.06	3.36
ethyl acetate	25.10	19.10	6.00	3.99	3.46	1-propanol	24.38	18.00	6.38	3.98	3.34
acetone	24.69	18.44	6.26	4.03	3.43	2-propanol	24.48	18.14	6.35	4.00	3.35
acetonitrile	24.59	18.14	6.45	4.06	3.42	butanol	24.43	18.00	6.43	4.02	3.38
DMSO	24.14	17.44	6.71	4.09	3.38	*tert*-butanol	24.66	18.48	6.18	3.92	3.37
formamide	23.83	17.38	6.45	4.13	3.39	EG	23.88	17.27	6.61	4.15	3.36

using some of the well-established solvatochromic scales proposed in the literature (vide infra). In doing so, useful information about the solute−solvent interactions in the ground and first excited singlet states can be obtained. This steady-state information would also give some indications about the intra- and/or intermolecular origin of the solvatochromic shifts, information which should be corroborated by the time-resolved measurements. To do so, one has to use a common measure for the solvatochromic shifts, and we have chosen to treat Stokes shifts as calculated from the mean frequencies (or the first moments) of fluorescence and absorption spectra. Fluorescence spectra were scaled by a λ^2 factor prior to the calculation of the mean frequencies. To obtain precise mean frequency values we fitted the spectra with a simplified log-normal function.[42]

$$\epsilon(\nu) = \epsilon_0 \exp\left(-\beta^2\left[\ln\frac{\nu - a}{b}\right]^2\right) \quad (1)$$

This simplified log-normal function allows the easy calculation of several important spectral parameters. In particular, the mean frequency and the fwhm of the spectrum are given by eqs 2−3.

$$\nu_{\text{mean}} = a + b \exp\left(\frac{3}{4\beta^2}\right) \quad (2)$$

$$\text{fwhm} = 2b \sinh\left(\frac{\sqrt{ln\,2}}{\beta}\right) \quad (3)$$

Resulting mean frequencies for the absorption and fluorescence spectra together with Stokes shifts of C151, C35, and C153 in various solvents are given in Tables 1a−c. The corresponding fwhm values for the absorption and fluorescence spectra are also given in Tables 1a−c.

Upon comparing our data for C153 with those of Maroncelli,[21] one can note that our absorption data are blue shifted by about 300 cm^{-1} and our fluorescence data are red shifted by about 300 cm^{-1}. The reason for this apparent discrepancy lies in the different methods used to evaluate the first moment of the spectra. Maroncelli and co-workers performed numerical integrations of the observed spectra, but over a limited interval for practical reasons (*i.e.*, for absorption spectra the high energy tail is omitted, while for emission spectra the low energy tail is missed). Our approach to fit the spectra with a log-normal function automatically includes the full band. This causes our observed Stokes shift to be about (600 ± 100) cm^{-1} larger than those of Maroncelli.[43]

Some general qualitative observations can be made prior to any quantitative analysis. Comparing the spectra (both absorption and fluorescence) of the three coumarins in a given solvent one sees clearly that the spectra shift to the red with increasing alkylation degree of the amino group (C151 < C35 < C153). This is due to the increased charge-transfer character of the excited S_1 state which has a stabilizing effect.[3] Both absorption and fluorescence spectra shift to the red with increasing solvent polarity, even if, as discussed below, the solvent polarity alone cannot account for all of the shift. Of particular interest is the red shift of the C151 absorption spectra when going from ethanol to water via methanol, which is also the case for C35 and C153. C151 was the only one of the three fluorinated coumarins which was soluble enough in water to get spectra. Interestingly, the opposite trend (also opposite to C1) was observed for C120.[3] It is likewise interesting to note the larger Stokes shifts observed for C151 (6200 to 7800 cm^{-1} water excluded) than for C35 (4400 to 7500 cm^{-1}) or C153 (4600 to 6800 cm^{-1}).

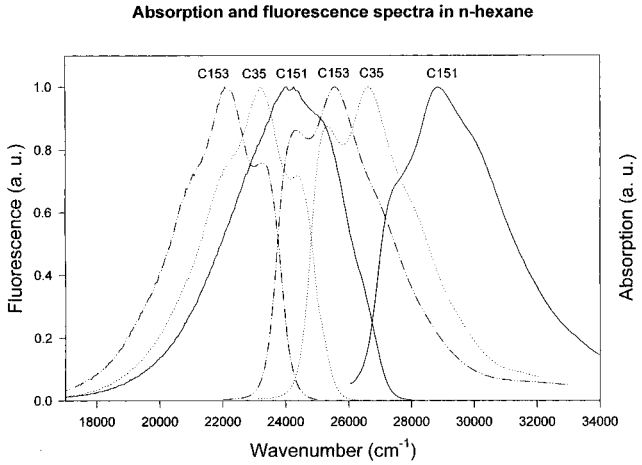

Figure 4. Absorption and fluorescence spectra of C151 (solid line), C35 (dotted line) and C153 (broken line) in *n*-hexane. It can be seen that the Franck−Condon factors are not favorable for the 0−0 transitions in either absorption or emission spectra. The figure shows also that there is no exact mirror symmetry between absorption and emission spectra and that there is a large difference in vibronic structure between C151 and the two other molecules.

In all solvents, except *n*-hexane, and to a certain extent diethyl ether, spectra are smooth and unstructured. Steady-state absorption and fluorescence spectra of C151, C35 and C153 in *n*-hexane are shown in Figure 4. From this figure it is clear that the Franck−Condon factors for the absorption and emission spectra are more intense for the ($\upsilon' \neq 0$) ← ($\upsilon'' = 0$) and ($\upsilon' = 0$) → ($\upsilon'' \neq 0$) transitions, respectively. What is more, this figure shows that there is only partial mirror symmetry between absorption and emission spectra. Interestingly, there is a large difference in vibronic structure between C151 and the two other molecules. From these observations, and particularly in the fluorescence spectrum of C151 in *n*-hexane, which exhibits a blurred and very broad structure, one may assume that a stronger intramolecular structural rearrangement occurs upon photoexcitation of C151.

It should be noted that the fwhm of the absorption and emission spectra are roughly equal in *n*-hexane for a given molecule. For all other solvents, the fwhm of the absorption spectrum increases with the observed Stokes shift, while the fwhm of the emission spectrum remains constant.[44] In the case of a linear solvation response, one would expect broadenings of the absorption and emission bands with increasing Stokes shift.[45] This is true for the absorption spectra of the three coumarins, but we observe the opposite for the emission spectra, which can be taken as an indication that the fluorescent excited-state solvation coordinate is not the same as for the ground state (i.e., an additional relaxation process must be taken into account).

Steady-state absorption and fluorescence spectra of the three 7-aminocoumarins C151, C35, and C153 in methanol and DMSO, for which time-resolved studies were performed, are shown in Figure 5. Also indicated (solid arrow) is the excitation frequency.

B. Solvatochromic Analyses of the Steady-State Stokes Shifts. The purpose of the solvatochromic study of steady-state Stokes shifts is to distinguish between solvent-induced shifts and spectral shifts due to intramolecular relaxation. This approach relies on the possibility to describe each solvent by one or several parameters reflecting the solvent effect on the spectral positions, band shapes, etc. This is of course far from trivial, but several parameters/scales have been proposed in the literature. The three solvatochromic scales we have used are

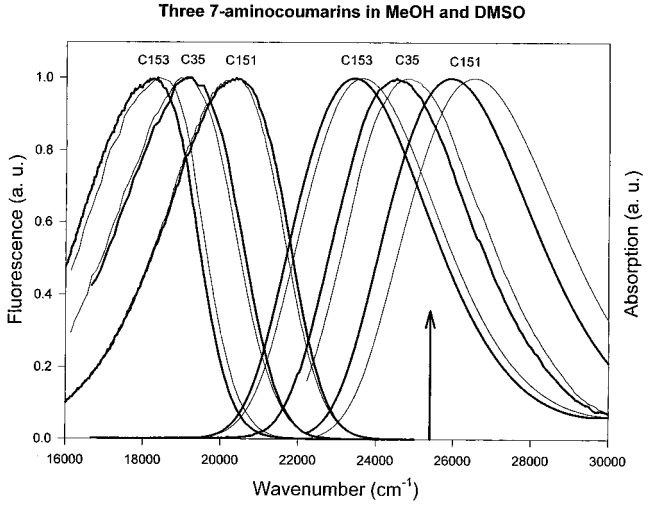

Figure 5. Steady-state absorption and fluorescence spectra of the three 7-aminocoumarins C151, C35, and C153 in methanol (thin solid lines) and dimethyl sulfoxide (thick solid lines). Also indicated (solid arrow) is the excitation frequency at 394 nm (=25380 cm^{-1}).

the Lippert parameter Δf,[46] the Dimroth parameter $E_T(30)$,[47,48] and the Kamlet and Taft (π^*, α, β) scale.[49−52]

The Lippert parameter Δf is constructed on theoretical grounds, to describe dielectric interactions due to polarity and polarizability. It is defined by the equation

$$\Delta f = \frac{\epsilon - 1}{2\epsilon + 1} - \frac{n^2 - 1}{2n^2 + 1} \tag{4}$$

where ϵ is the dielectric constant and n the refractive index. This parameter connects the Stokes shift to the change in dipole moment between the ground and the excited state, $\Delta\mu = (\mu_e - \mu_g)$, of the solute by the following equation

$$\Delta\upsilon = \Delta\upsilon_0 + \frac{2}{hca^3}(\mu_e - \mu_g)^2 \Delta f \tag{5}$$

where a is the radius of the spherical cavity approximating the solute. In the calculations, values for ϵ and n were taken from the tables of Riddick et al.[53]

The Dimroth parameter $E_T(30)$ is simply calibrated against the observed solvatochromic shifts of the charge-transfer betaine molecule.

While the Lippert parameter Δf and the Dimroth parameter $E_T(30)$ are both indicators of basically the solvent bulk dielectric properties, the Kamlet and Taft scale (π^*, α, β) takes explicitly hydrogen bonds into account. In a series of papers, Kamlet, Taft, and co-workers[51,52] developed an empirical model describing the solvent effects on the steady-state absorption or emission spectra. According to this model, a given spectral observable XYZ may be parametrized as

$$\mathrm{XYZ} = \mathrm{XYZ}_0 + s\pi^* + a\alpha + b\beta \tag{6}$$

XYZ may be the peak or the mean frequency of the absorption or emission spectrum or any other solvent-sensitive observable. Applied to the steady-state Stokes shift, the generalized solvatochromic equation is

$$\Delta\upsilon = \Delta\upsilon_0 + \Delta s\pi^* + \Delta a\alpha + \Delta b\beta \tag{7}$$

In this formula π^* is the polarity/polarizability parameter of the solvent, α is the index of hydrogen bond donor (HBD) character of the solvent (acidity), and β is the index of hydrogen

TABLE 2: Various Solvent Parameters Used in the Solvatochromic Studies. Values for the Lippert Parameter Δf were Calculated from ϵ and n_D Values Taken from Ref 53, $E_T(30)$ Values Were Taken from Ref 48, and π^*, α, β Values were Taken from Refs 51 and 52

solvent	Δf	$E_T(30)$	π^*	α	β
n-hexane	−0.0005	31.0	−0.08	0.00	0.00
diethyl ether	0.1669	34.5	0.27	0.00	0.47
THF	0.2096	37.4	0.58	0.00	0.55
1,4-dioxane	0.0204	36.0	0.55	0.00	0.37
ethyl acetate	0.2002	38.1	0.55	0.00	0.45
acetone	0.2846	42.2	0.71	0.08	0.48
acetonitrile	0.3046	45.6	0.75	0.19	0.31
DMSO	0.2630	45.1	1.00	0.00	0.76
formamide	0.2822	55.8	0.97	0.71	0.48
DMF	0.2744	43.2	0.88	0.00	0.69
DMA	0.2724	42.9	0.88	0.00	0.76
methanol	0.3086	55.4	0.60	0.93	0.62
ethanol	0.2887	51.9	0.54	0.83	0.77
1-propanol	0.2741	50.7	0.52	0.78	0.80
2-propanol	0.2762	48.4	0.48	0.76	0.95
1-butanol	0.2635	49.7	0.47	0.79	0.88
tert-butanol	0.2514	43.3	0.41	0.68	1.01
EG	0.2745	56.3	0.92	0.90	0.52
water	0.3201	63.1	1.09	1.17	0.18

bond acceptor (HBA) character of the solvent (basicity). $\Delta\nu_0$ is the difference of the frequencies of the peaks or the barycenters of the absorption and emission spectra in the case of zero solute−solvent interaction (i.e., the purely intramolecular contribution), Δs is the difference of the susceptibilities of the solute property to changing solvent polarity-polarizabilities between S_1 and S_0, Δa is the difference of the susceptibilities of the solute property to changing solvent hydrogen bond donor character between S_1 and S_0, and Δb is the difference of the susceptibilities of the solute property to changing solvent hydrogen bond acceptor character between S_1 and S_0.

The values of Δf, $E_T(30)$, and (π^*, α, β) for the different solvents used are given in Table 2.

From our data it is clear that the observed Stokes shifts are not correlated with the $E_T(30)$ parameter. This is not surprising in view of the large difference between the structures of coumarin and betaine molecules.

The Lippert parameter Δf leads to rather good correlations for C35 and C153, but less so for C151. From the slopes of these linear regressions and with the solute radius a calculated from the van der Waals volumes, using eq 5 we obtain estimations of the $\Delta\mu$ for the three coumarins: $\Delta\mu$(C151) = 4.6 D, $\Delta\mu$(C35) = 6.6 D, and $\Delta\mu$(C153) = 6.0 D. For C35 and C153 these values are in agreement with previously reported values of $\Delta\mu$ when calculated in the same way[4,31] (for example, $\Delta\mu$(C153) = 6.0 D[4]). For C153, a $\Delta\mu$ = 4.1 D was obtained using a different reaction field parameter.[21] For C151, which is substituted by primary amino groups, the accordance is worse, which is not surprising since the poor regression is due to hydrogen bonding solvents.[31]

The best correlation between experimental and calculated Stokes shift data is obtained using the Kamlet and Taft framework,[29,49] which explicitly takes into account hydrogen bonding properties of both solvent and solute. Thus, in the following we will concentrate on the Kamlet and Taft treatment. Resulting fits for the three coumarins are shown in Figure 6a−c, where calculated Stokes shifts are plotted against observed ones. The parameters resulting from these fits are given in Table 3.

In no case could dioxane data be properly reproduced. We have therefore excluded dioxane from the fits presented in Table 3. The peculiar behavior of coumarins in dioxane was already noted by Rechthaler and Köhler.[31] Dioxane is a hydrogen bond acceptor ether which seems to have the polarity of diethyl ether in Brooker's χ_R scale[54] and that of ethyl acetate or tetrahydrofuran in the Kamlet and Taft scale.[49] For the two coumarins C35 and C153, formamide data could not be used, which may point toward some specific interaction, or just that the Kamlet and Taft model breaks down for this solvent which is extremely polar and with strong HBD and HBA character. For C153 finally, ethylene glycol data had to be excluded as well. Actually, looking at the C151 fit, one sees that formamide and ethylene glycol data are slightly off the line too, but this is "hidden" by the relatively good fit when including the far-off water data point. It may be so that water is badly described by the Kamlet and Taft treatment, in which case the deviations of formamide and ethylene glycol would stick out much more. To conclude, the Kamlet and Taft fits are far from perfect, but we believe that they are good enough to draw some interesting conclusions, and that the fits are much more reliable than both the Lippert and the Dimroth parameters.

TABLE 3: Solute Parameters Resulting from the "Kamlet and Taft" Analysis of the Steady-State Stokes Shifts (Mean Frequencies) of Coumarins C151, C35, and C153 in a Number of Solvents (17 for C151, 16 for C35, and 15 for C153). All Quantities in Units of 10^3 cm^{-1}

	C151	C35	C153
$\Delta\nu_0$	6.50 ± 0.13	4.90 ± 0.12	4.85 ± 0.06
Δs	1.28 ± 0.14	2.09 ± 0.17	1.83 ± 0.09
Δa	0.90 ± 0.10	0.88 ± 0.11	0.86 ± 0.06
Δb	−0.88 ± 0.16		

Using the solute dependent parameters given by the Kamlet and Taft treatment in Table 3 and referring to the chemical structures given in Figure 1, following Arbeloa et al.,[3] some interesting conclusions can be made regarding the changes in specific solute−solvent interactions. For all three coumarins, there is a stabilizing term, $\Delta a > 0$, of the excited state by accepting hydrogen bonds from the solvent. This effect is actually the resultant of two effects, namely the decrease of the strength of the hydrogen bond (Type A) and the increase of the hydrogen bond strength (Type B) (see Figure 1). The strengthening of the hydrogen bond on the carbonyl group is thus stronger than the weakening of the hydrogen bond on the nitrogen lone pair. For C151, there is an additional destabilizing term, $\Delta b < 0$, of the excited state by the weakening of the hydrogen bonds (Type C) (see Figure 1). For this coumarin the net effect of the specific interaction will be roughly zero for a solvent which is equally hydrogen bond donating and accepting. Interestingly, the weakening of (type C) hydrogen bonds in the case of C151 is contrary to the ideas of Arbeloa et al.[3] who stated that interactions B and C are more important in the first excited state. In fact, the $b\beta$ term in eq 6 is negative for both the absorption and fluorescence frequencies but its absolute value is smaller in fluorescence than in absorption. This is also the case of C120.[55]

C. Estimation of the Solvent-Induced Spectral Shifts. The Kamlet and Taft treatment and the solute parameters obtained allow us now to calculate the pure solvent contribution to the Stokes shift in a given solvent, this being the sum of the three terms $\Delta s\pi^*$, $\Delta a\alpha$, and $\Delta b\beta$. The resulting values are given in Table 4.

The aim of this treatment is to have an independent estimation of the solvent contribution to the time-dependent Stokes shift, which can be compared to experimental data from time-resolved measurements (vide infra). Other ways to obtain such a measure have been proposed by Maroncelli et al., who conceived a very

TABLE 4: Calculated Solvent Contributions to the Steady-State Stokes Shifts of the Three Coumarins C151, C35, and C153 in Methanol and DMSO[a]

	$\Delta\nu_{Stokes}$ (K&T)	$\Delta\nu_{Stokes}$ (Δ(*n*-hexane))
C151/MeOH	1.05	1.54
C35/MeOH	2.07	2.70
C153/MeOH	1.90	2.11
C151/DMSO	0.60	0.89
C35/DMSO	2.10	2.46
C153/DMSO	1.83	2.04

[a] In the second column are the values calculated from the "Kamlet and Taft" analysis. In the last column are the increases relative to the observed Stokes shift in *n*-hexane. All frequencies in units of 10^3 cm^{-1}.

detailed but fairly complex method to estimate the time-zero emission spectra from steady-state data.[17] They applied this method to time-resolved measurements of the fluorescence spectra of coumarin C153 in various solvents.[21,22] In these papers they also proposed a much easier way to obtain the same measure. By simply subtracting the Stokes shift observed in a nonpolar aprotic solvent from the Stokes shift observed in the solvent under study, one gets a rough estimate of the solvent contribution. This implies that the Stokes shift in the nonpolar, aprotic solvent is independent of the solvent (i.e., intramolecular). As a nonpolar, aprotic solvent Maroncelli used 2-methylbutane, but *n*-hexane should serve equally well in our case. We have used this method to calculate the solvent contribution to the observed Stokes shifts in methanol and DMSO by simply subtracting the Stokes shift in *n*-hexane. The resulting solvent contributions given in Table 4 show that the two estimates follow the same trend although the calculated ones using the Kamlet and Taft treatment are smaller by about 30%.

However, we choose to estimate the solvent contribution to the TDFSS using the Kamlet and Taft treatment for the following reasons. First, it is rather difficult to get a good estimate of the mean frequency of the absorption and emission spectrum of a coumarin in the nonpolar and aprotic *n*-hexane. The spectra display fairly clear vibrational structure as described above. Second, the results from the Kamlet and Taft treatment are based on the evaluation of the Stokes shift in many different solvents and are thus considered to be more accurate.

IV. Time-resolved Spectra: Results and Analysis

A. Raw Data Treatment. Spectra were corrected for the spectral response of the upconversion detection system in a multistep process, based on the comparison with a steady-state fluorescence spectrum. We will describe this process more in detail in the following.

First of all, it is important to subtract the background from the time-resolved upconversion spectra. The background was recorded by positioning the delay at "negative" time (i.e., so that the gating pulse arrives to the upconversion crystal well before the fluorescence). In this manner one can be sure that all residual noise contributions from the noninteracting fluorescence and the gating pulse plus the room are measured correctly. The same integration time was used for the background as for all other recordings, and several acquisitions were averaged in order to improve the statistics.

Second, time-resolved spectra were corrected for the spectral response of the detection system. This response curve depends on various physical parameters such as the color filters used, the monochromator grating, the spectral sensitivity of the photomultiplier tube, etc., but also on the spatial overlap between the gating laser pulse and the fluorescence inside the BBO crystal. When tuning the fluorescence wavelength, the phase matching angle of the sum frequency generation crystal must be changed which induces a change in the overlap of the two beams. For this last reason, it is practically impossible to calculate the true correction curve. Instead, the "current" spectral correction curve was determined experimentally by comparing, as described below, the fluorescence upconversion spectrum at long times (500 ps) with the steady-state spectrum recorded for the same solution[56] and corrected for the response function of the conventional spectrofluorometer.

Once the "infinite time" spectrum is recorded and the background subtracted from this as well, the resulting spectrum $I^{\infty}(\lambda)$ was compared to the steady-state spectrum $I^{SS}(\lambda)$. Both spectra, defined on a wavelength scale, were normalized, whereafter the ratio

$$R(\lambda) = \frac{I^{SS}(\lambda)}{I^{\infty}(\lambda)} \tag{8}$$

was calculated. This ratio is well defined in the wavelength region where the two spectra are individually well defined. However, in the blue wing, and to a lesser extent in the red wing, the ratio becomes less well characterized, so the calculated $R(\lambda)$ function was smoothed by an empirical function (a double-sided polynomial). Moreover, for very short wavelengths, where the system's spectral response is limited by the filters (GG420 and UG11), $R(\lambda)$ was extrapolated by the inverse of the transmission curve of the filters.

All time-resolved spectra were subsequently multiplied by the correction curve. 3D-views of the time-resolved emission spectra of C151, C35, and C153 in methanol and DMSO are shown in Figure 7a and b.

B. Analysis of the Temporal Evolution of the Fluorescence Spectra and Results. Before any further treatment, time-resolved fluorescence spectra were transformed to frequency-scale and therefore scaled by a λ^2 factor. As described above for the treatment of steady-state spectra, mean frequencies of the time-resolved spectra were obtained by fitting them with the log-normal function defined by eq 1. This procedure has been adopted with success in the treatment of time-resolved spectra,[39] where a reliable interpolation and "smoothing" of a small number of data points is needed, and in particular in the "spectral reconstruction" method concerning time-resolved emission spectra as elaborated by Maroncelli and Fleming.[4]

This treatment enables an easy visualization of characteristic spectral parameters against time, without imposing any particular functionality. Such a first visualization is important in order to find appropriate analytical expressions for the time dependencies of the parameters. An example of the resulting spectral fits is given in Figure 8, where observed spectra and fitted log-normal functions for C35 in methanol can be seen.

This treatment is, however, not fully satisfying since the pulses are finite in time and the temporal overlap extends for several hundreds of femtoseconds (*i.e.*, the response function of 200 fs fwhm described above). Evidently, to extract the valid information, data need to be deconvoluted.[57] In the standard procedure,[4] separate kinetic traces are fitted before the spectral reconstruction, thus introducing independent and hypothetical time-zeroes for each experimental trace but furnishing model functions from which the authors deduced time-resolved fluorescence spectra. In our case, however, deconvolution of experimental data means fitting the full three-dimensional surface which may be an easy task numerically speaking, but will definitely be sorely sensitive to the choice of the model function describing the model intensity surface in time and wavenumber.

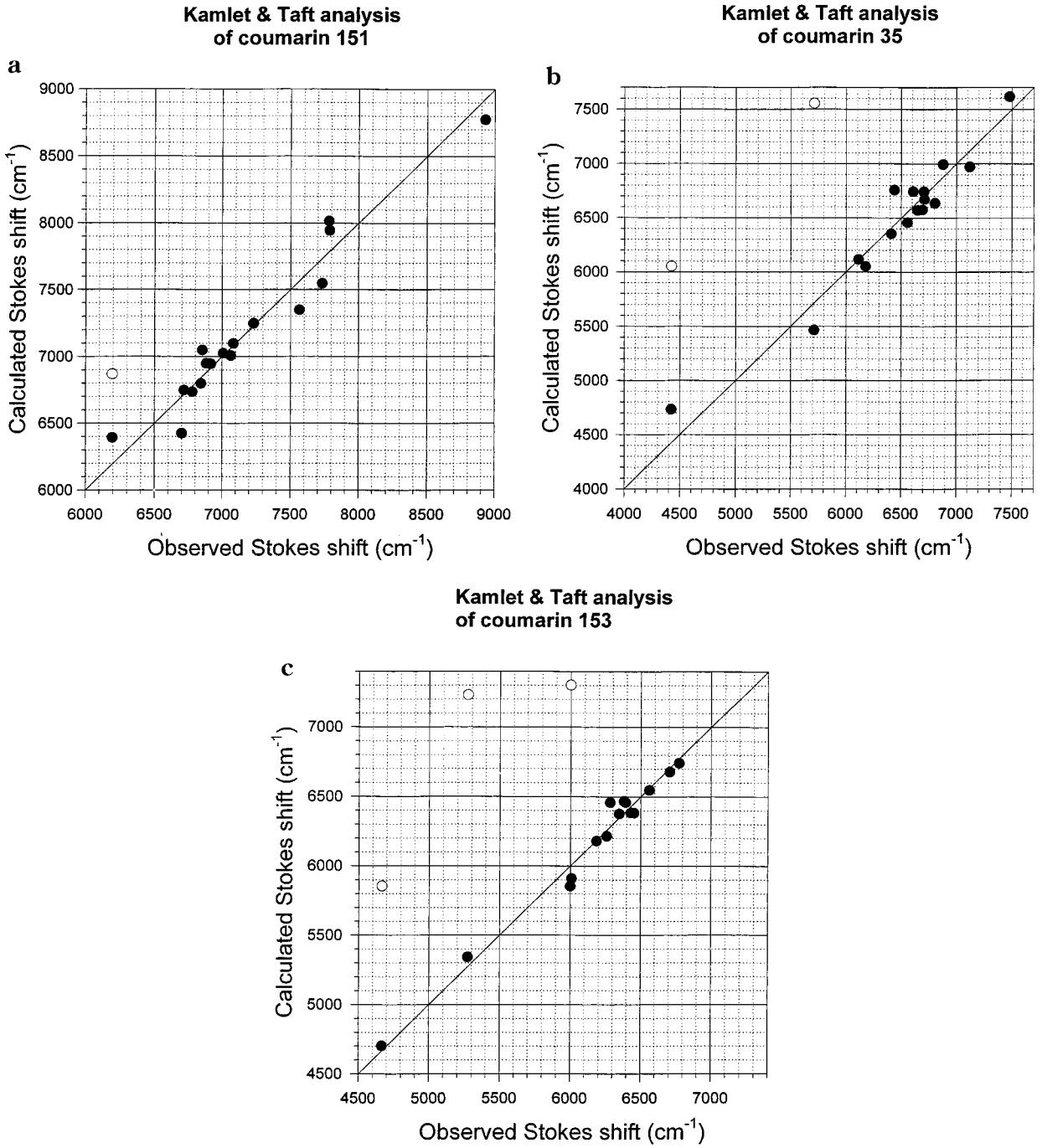

Figure 6. (a) Observed steady-state Stokes shifts (based on the average frequencies of absorption and fluorescence spectra, see Table 1a for a listing of data) of coumarin C151 versus calculated Stokes shifts using the Kamlet and Taft (π^*, α, β) scale. 17 solvents were used in the fit (filled circles, see Table 3 for the resulting parameters). Dioxane (open circle) was excluded from the fit. (b) Observed steady-state Stokes shifts (based on the average frequencies of absorption and fluorescence spectra, see Table 1b for a listing of data) of coumarin C35 versus calculated Stokes shifts using the Kamlet and Taft (π^*, α, β) scale. 16 solvents were used in the fit (filled circles, see Table 3 for the resulting parameters). Dioxane and formamide (open circles) were excluded from the fit. (c) Observed steady-state Stokes shifts (based on the average frequencies of absorption and fluorescence spectra, see Table 1c for a listing of data) of coumarin C153 versus calculated Stokes shifts using the Kamlet and Taft (π^*, α, β) scale. Fifteen solvents were used in the fit (filled circles, see Table 3 for the resulting parameters). Dioxane, formamide, and EG (open circles) were excluded from the fit.

We will now describe a new alternative way to treat observed TDFSS data. First of all, let us note that all our TDFSS (time-dependent fluorescence Stokes shift) data refer to the mean frequency of the time-resolved fluorescence spectrum as calculated by eq 2. We will define the TDFSS as

$$\delta\bar{\nu}(t) = \bar{\nu}(t) - \bar{\nu}(\infty) \tag{9}$$

In the following, we want to distinguish clearly between this observed TDFSS and the "real" mean frequency dynamic Stokes shift (rMFDSS).[58] The observed TDFSS should be seen as the convolution between the rMFDSS function and the experimental response function of the system. In analogy with eq 9 we can thus write rMFDSS as

$$\Delta\bar{\nu}(t) = \bar{\nu}'(t) - \bar{\nu}'(\infty) \tag{10}$$

where now the primed mean frequencies are calculated from the nonconvoluted model function intensity surface. To obtain the "real" mean frequency we have developed and applied a

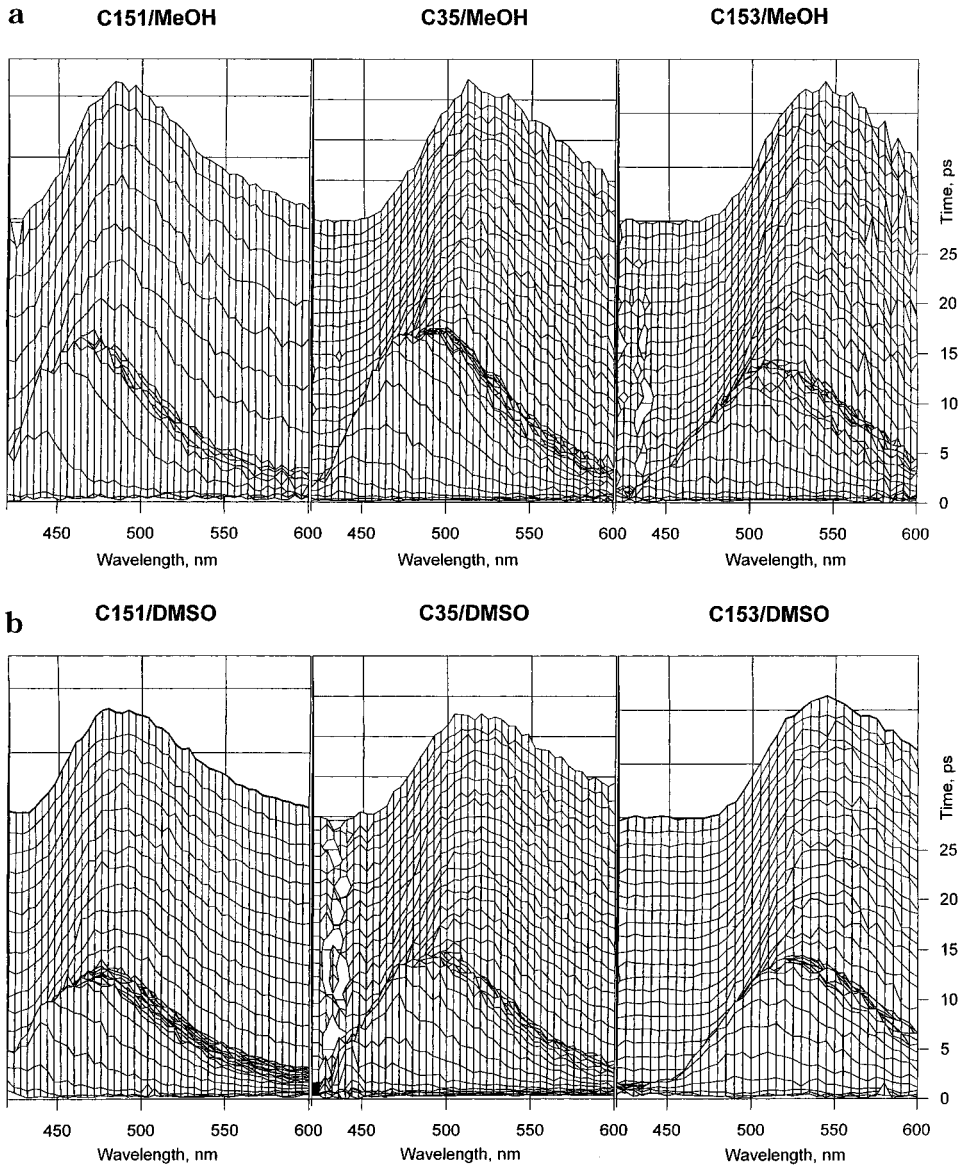

Figure 7. (a) Three-dimensional view of the time-resolved fluorescence spectra of C151, C35, and C153 in methanol. (b) Three-dimensional view of the time-resolved fluorescence spectra of C151, C35, and C153 in DMSO.

procedure, which treats the results obtained from the log-normal fitting of raw time-resolved spectra described in the preceding paragraph. This procedure is actually based on iterative nonlinear fittings/deconvolutions of the integrated fluorescence intensity $I(t)$ and the product $\delta\bar{\nu}(t)I(t)$. This merged fitting gives the nonconvoluted rMFDSS model function $f(t)$ and fluorescence intensity profile $i(t)$. This procedure is described in detail in the Appendix. In the treatment the infinite-time value of the mean-frequency $\bar{\nu}(\infty)$ was fixed to the value obtained for the steady-state spectra (see Table 1).

The deconvolution allows the determination of the zero-time, perfectly characterized by the rise of the integrated intensity, and enables us to have a higher precision in the model description of the dynamic Stokes shift. Since input data are sampled with different time-steps (typically 20 spectra with 67 fs steps, covering the interval from negative times to just beyond the rise due to the convolution, followed by 20 spectra with a 20 times longer time-step (i.e., 1.33 ps)) input data were interpolated with the smaller time-step. Accordingly, all data points corresponding to the long time-step were weighted down with a factor $\sqrt{20}$ in the fitting procedure, to give an equal importance to the fast and the slow contributions of the TDFSS.

As described in the Appendix, the rMFDSS is described by a triexponential model function:

$$\Delta\bar{\nu}(t) = \Delta\bar{\nu}[\alpha e^{-t/\tau_1} + \beta e^{-t/\tau_2} + \gamma e^{-t/\tau_3}] \qquad (11)$$

A triexponential model function was found necessary, but in all cases the shortest component (τ_1) was faster than the shortest sampling step of 67 fs and therefore fixed to 50 fs in the fitting procedure, corresponding to the experimental time resolution.

An example of the merged fitting of the time-dependent fluorescence Stokes shift $\delta\bar{\nu}(t) = \bar{\nu}(t) - \bar{\nu}(\infty)$ (actually the product $\delta\bar{\nu}(t)I(t)$) and the integrated fluorescence intensity $I(t)$ is given in Figure 9a and b where observed and fitted curves for C151 in DMSO are shown. As can be seen the agreement between experimental and model calculated data is very good. The model reproduces very well the rapid evolution observed within the first picosecond but also the longer time evolution up to 45 ps. The intensity rise time was found to be instantaneous within our experimental resolution ($\ll$200 fs). The corresponding fitted triexponential rMFDSS model function is shown in Figure 10. Note the ultrafast component, the amplitude of which is about 60% of the total shift. The total

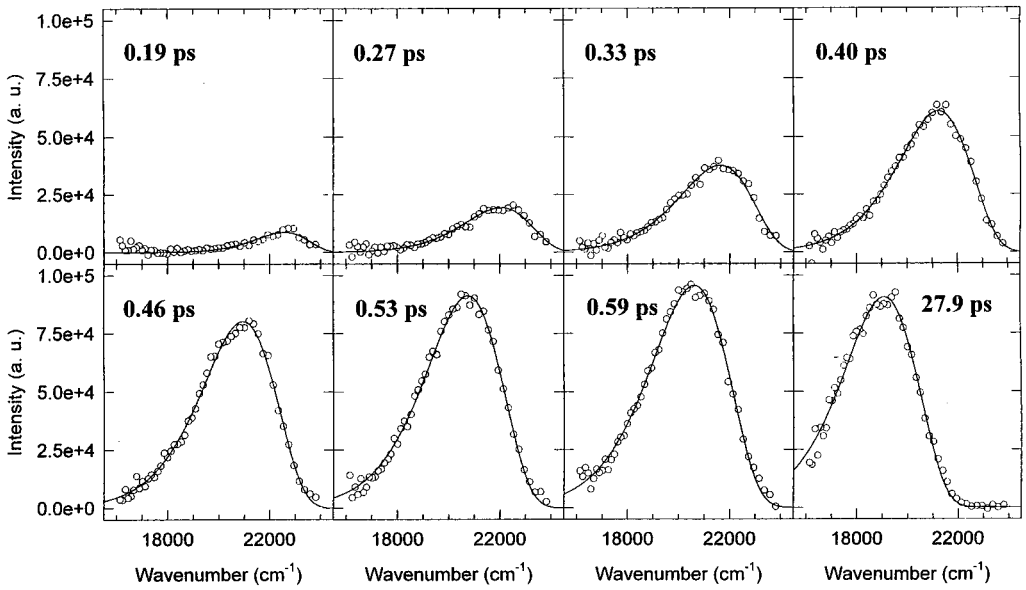

Figure 8. Observed and log−norm-fitted time-resolved fluorescence spectra of C35 in methanol.

amplitude of the rMFDSS is somehow correlated to the fact that we have fixed the fast time to 50 fs. This may be an overestimation of the actual value, but if it is shorter, the relative amplitude will only increase. Resulting parameters from the fitting of time-resolved spectra for C151, C35, and C153 in methanol and DMSO are given in Tables 5−6.

To compare results it is usual to use the normalized spectral shift functions $c(t)$ defined by eq 12 using the notation in the Appendix.[59]

$$c(t) = \frac{\Delta\bar{\nu}(t)}{\Delta\bar{\nu}(0)} \tag{12}$$

The calculated $c(t)$ functions for the three coumarins C151, C35, and C153 in MeOH and DMSO are given in the captions of Tables 5−6 and shown in Figure 11. We would like to make a caution at this point about the errors given in Tables 5−6. The values given in the tables correspond to one standard deviation in the numerical fit, but the real uncertainties are definitely much larger, we estimate them to at least 10%. Now, comparing the different results, the most striking feature is the clear difference of the dynamics found in methanol and DMSO. More interestingly, two simple observations can be made about the dynamics: first, even though there are subtle differences between the different coumarins in a given solvent, we do not judge them as significant, second, in both methanol and DMSO the relaxation is dominated by an ultrafast component, accounting for about 60% of the total relaxation in methanol and about 70% in DMSO. Also shown as an insert in Figure 11, is the slow part of the $c(t)$ function, $c_{slow}(t)$ defined by

$$c_{slow}(t) = \frac{\beta e^{-t/\tau_2} + \gamma e^{-t/\tau_3}}{\beta + \gamma} \tag{13}$$

where the parameters were fixed to values given in Figures 5 and 6. From this figure it seems that there is less effect of the solute in DMSO than in MeOH. However, the small differences observed in MeOH have to be taken with caution.

C. Comparison between Time-Resolved and Steady-State Stokes Shifts. As outlined in the Introduction, the aim of the present study is double. One partial aim is to try to elucidate the nature of the ultrafast component so often observed in femtosecond studies of solvation dynamics and in particular in our data. The other partial aim is to address the influence of the breaking and remaking of hydrogen bonds on the observed spectral shifts.

Our intentions are now to compare the information obtained from the steady-state measurements and the solvatochromic analyses of the Stokes shifts with the results from the time-resolved studies. As a starting point we compare the total observed Stokes shifts for the three coumarins in methanol and DMSO obtained from the time-resolved measurements (Tables 5 and 6) with the corresponding values predicted with the analysis based on the Kamlet and Taft scales (Table 4). This comparison is shown in Figure 12 (open symbols: MeOH, circles; DMSO, squares). As can be seen, the time-resolved total shifts are always much larger (about a factor of 2) than the predicted values. This implies that the shifts predicted using the Kamlet and Taft analysis seem to miss a nonnegligible part of the Stokes shift. In other words, apart from the solvent relaxation there must be other, presumably intramolecular, contributions to the total observed dynamic Stokes shift. These intramolecular contributions can be of electronic origin, rapid vibrational relaxation, or related to a geometric change of the coumarin dye molecule as briefly discussed in the Introduction.[3]

Remembering that our deconvolution/fits of $c(t)$ using triexponential model functions resulted in an unresolvably fast component (fixed to 50 fs) which accounted for 60−70% of the total Stokes shift, we will now make a distinction between this "ultrafast" component and the "slow" part of the measured time-dependent shift associated with τ_2 and τ_3. If we take only the slow part of the shift, as opposed to the total shift, and compare these values with the KT predictions a completely different picture is obtained as shown in Figure 12 (filled symbols: MeOH, circles; DMSO, squares). The amplitudes of the "slow" part for the six measurements are given in Tables 5 and 6. While there is a close resemblance between observed "slow" fluorescence shifts and predictions according to the "Kamlet and Taft" description for C151, this is not the case for C35 and C153. For these coumarins the "slow" parts of the observed fluorescence shifts are not able to account for all of the predicted solvent-induced shifts.

So which of the two comparisons is the most instructive one? Comparing "Kamlet and Taft" predictions with the whole Stokes

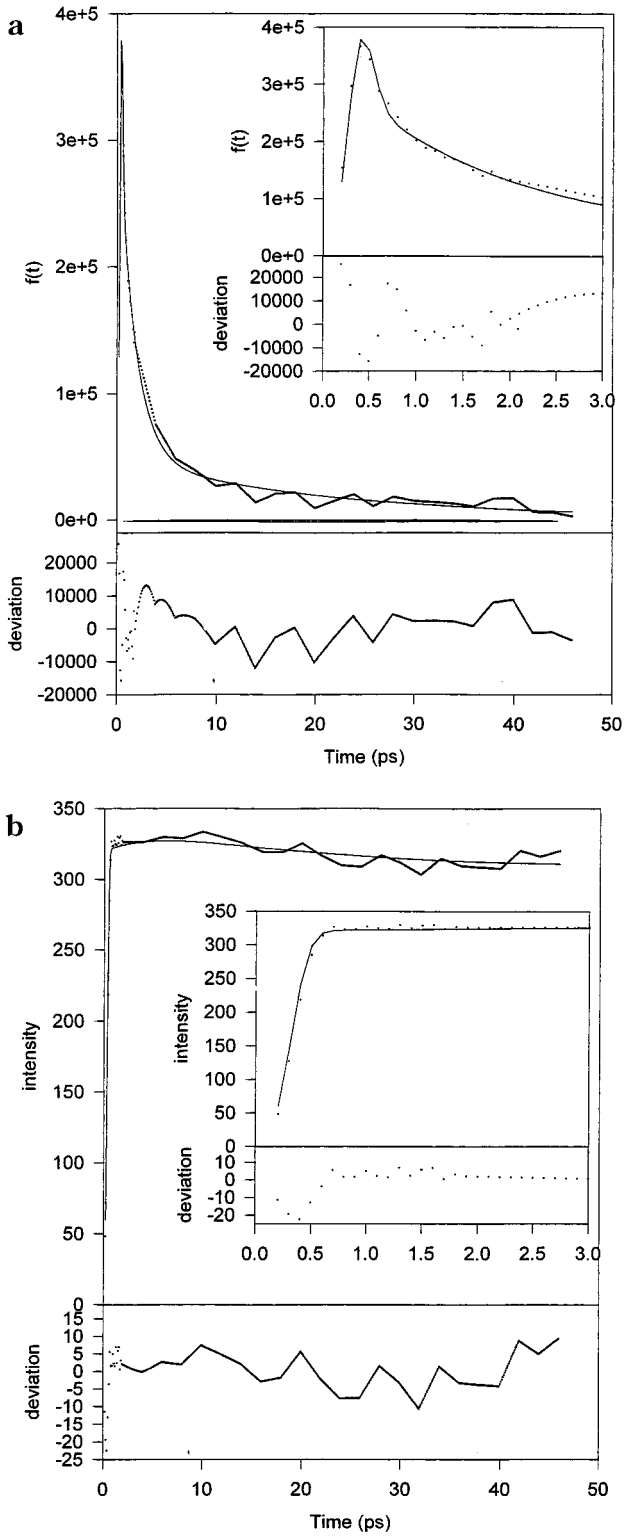

Figure 9. (a) An example of the merged fitting of the time-dependent fluorescence Stokes shift $\delta\bar{\nu}(t) = \bar{\nu}(t) - \bar{\nu}(\infty)$ and the integrated fluorescence intensity $I(t)$ for C151 in DMSO. The fit is actually based on a merged iterative nonlinear fitting/convolution of $I(t)$ and the product $\delta\bar{\nu}(t)I(t)$ (see the Appendix). Shown here are observed and fitted $\delta\bar{\nu}(t)I(t)$ curves. As can be seen, the agreement between experimental and model data is very good. (b) As in Figure 9a with the difference that observed and fitted $I(t)$ curves are shown.

shift observed or only the slow part? In the following we will argue for the latter one.

Going back to Figure 11 we observe that there is no significant difference between the rMFDSS of C151 and the

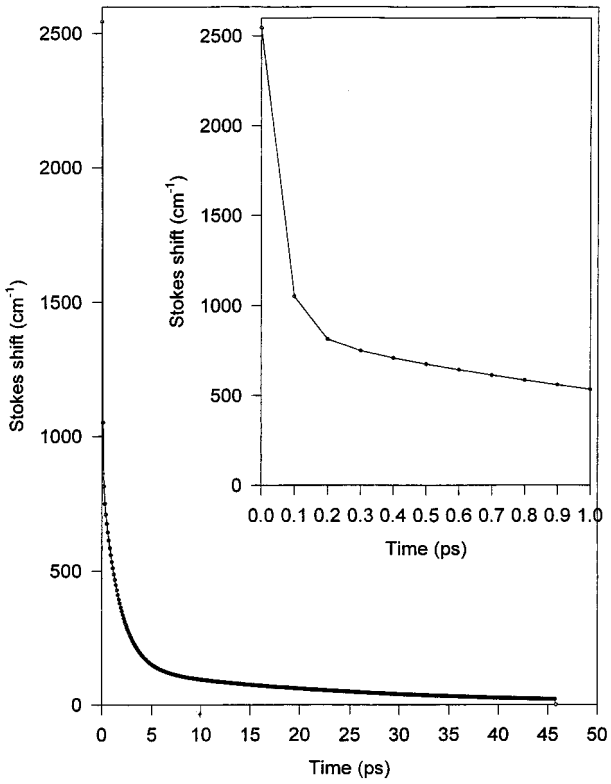

Figure 10. Example of a triexponential model function used to describe the real mean frequency dynamic Stokes shifts function rMFDSS $f(t)$. This particular function is the one corresponding to the fit for C151 in DMSO as shown in Figure 9a and b.

TABLE 5: Resulting Parameters from the Deconvolution/Fit of the Temporal Evolution of the Mean Frequency of C151, C35, and C153 in Methanol Using a Triexponential Model Function[a]

	C151	C35	C153
$\bar{\nu}_\infty$[b]	19604	18357	17487
$\Delta\bar{\nu}(0)$	2604 ± 21	3182 ± 20	2655 ± 36
τ_1[c]	0.050	0.050	0.050
τ_2	2.28 ± 0.11	1.05 ± 0.04	3.36 ± 0.29
τ_3	15.48 ± 0.41	11.17 ± 0.13	20.13 ± 1.85
α	0.558 ± 0.006	0.519 ± 0.006	0.546 ± 0.008
β	0.237 ± 0.007	0.203 ± 0.004	0.262 ± 0.017
γ	0.204 ± 0.007	0.278 ± 0.005	0.191 ± 0.017
$\langle\tau\rangle$	3.73 ± 0.14	3.34 ± 0.06	4.76 ± 0.50
$\tau_{1/e}$	0.716	0.679	1.128
$\Delta\bar{\nu}_{slow}$	1151	1531	1205

[a] The function is of the form $\Delta\bar{\nu}(t) = \Delta\bar{\nu}c(t) = \Delta\bar{\nu}(0)[\alpha e^{-t/\tau_1} + \beta e^{-t/\tau_2} + \gamma e^{-t/\tau_3}]$. The values given in the tables correspond to one standard deviation in the numerical fit, but the real uncertainties are definitely much larger; we estimate them to at least 10%. [b] $\bar{\nu}_\infty$ was fixed to the value calculated from the steady-state spectrum. [c] τ_1 was fixed to 50 fs, the shortest possibly observable value after deconvolution.

two other coumarins studied in a given solvent although this coumarin is also a hydrogen bond donor (type C, see Figure 1) as shown using the Kamlet and Taft solvent scales. This lack of discrimination may seem surprising in view of the marked difference between the steady-state solvatochromisms of C151 and the two other molecules (see Table 3).

Let us briefly recall the different hydrogen bonds involved. Both coumarins C35 and C151 may accept hydrogen bonds at the nitrogen lone pair (type A) and the carbonyl group (type B) from hydrogen bond donating solvents. Only C151 may establish hydrogen bonds with hydrogen bond accepting solvents from the two H-atoms on the amino group (type C). This leads us to distinguish four different situations upon coumarin

TABLE 6: Resulting Parameters from the Deconvolution/Fit of the Temporal Evolution of the Mean Frequency of C151, C35, and C153 in DMSO Using a Triexponential Model Function[a]

	C151	C35	C153
$\bar{\nu}_\infty$[b]	19647	18388	17357
$\Delta\bar{\nu}(0)$	2545 ± 20	3121 ± 15	2194 ± 14
τ_1[c]	0.050	0.050	0.050
τ_2	1.68 ± 0.05	2.07 ± 0.05	2.29 ± 0.05
τ_3	23.47 ± 1.77	16.03 ± 1.04	29.68 ± 3.43
α	0.659 ± 0.005	0.638 ± 0.003	0.625 ± 0.004
β	0.286 ± 0.006	0.300 ± 0.005	0.345 ± 0.004
γ	0.055 ± 0.004	0.062 ± 0.004	0.030 ± 0.003
$\langle\tau\rangle$	1.80 ± 0.13	1.64 ± 0.09	1.71 ± 0.13
$\tau_{1/e}$	0.130	0.156	0.176
$\Delta\bar{\nu}_{slow}$	868	1130	823

[a] The function is of the form $\Delta\bar{\nu}(t) = \Delta\bar{\nu}c(t) = \Delta\bar{\nu}(0)[\alpha e^{-t/\tau_1} + \beta e^{-t/\tau_2} + \gamma e^{-t/\tau_3}]$. The values given in the tables correspond to one standard deviation in the numerical fit, but the real uncertainties are definitely much larger; we estimate them to at least 10%. [b] $\bar{\nu}_\infty$ was fixed to the value calculated from the steady-state spectrum. [c] τ_1 was fixed to 50 fs, the shortest possibly observable value after deconvolution.

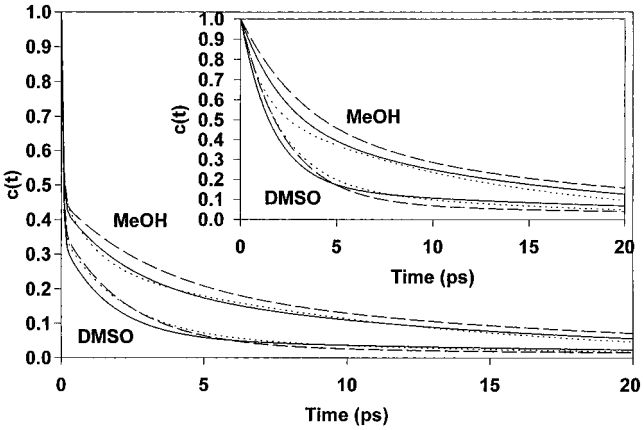

Figure 11. Normalized real mean frequency dynamic Stokes shifts functions rMFDSS $f(t)$ for the three coumarins C151 (solid lines), C35 (dotted lines), and C153 (broken lines) in MeOH and DMSO, described by the fitted triexponential model functions. Also shown as an insert is the normalized slow part of the $c(t)$ function, corresponding to only the τ_2 and τ_3 terms of the model function.

photoexcitation: (1) C151/MeOH, 3 hydrogen bonds are broken, 1 is formed; (2) C151/DMSO, 2 hydrogen bonds are broken; (3) C35,C153/MeOH, 1 hydrogen bond is broken, 1 is formed; (4) C35,C153/DMSO, no hydrogen bonds.

After having discussed the nature of the different hydrogen bonds involved, let us now turn to their dynamics. Actually, a good starting point is a comment about time scales made by Phelps et al.[60] in their work on molecular dynamics simulations of solvation in methanol. "The shorter time scale for dissipating, as opposed to creating, the polarized solvation sphere may be rationalized on the bases of the anticipated case of dissociating a relatively ordered solvent structure as compared to forming it, i.e. on entropic grounds." A similar conclusion has been reached by Fonseca and Ladanyi[61] and by Skaf and Ladanyi[62] who investigated the solvation and hydrogen bond dynamics in methanol and in methanol−water mixtures using molecular dynamics simulations. The breakage of the solute−solvent hydrogen bond was found to occur much faster than the formation of it. Some care is, however, required in interpreting these results since the simulations were carried out for idealized dipolar solutes whose charge distribution is quite unlike that of a Coumarin dye molecule.

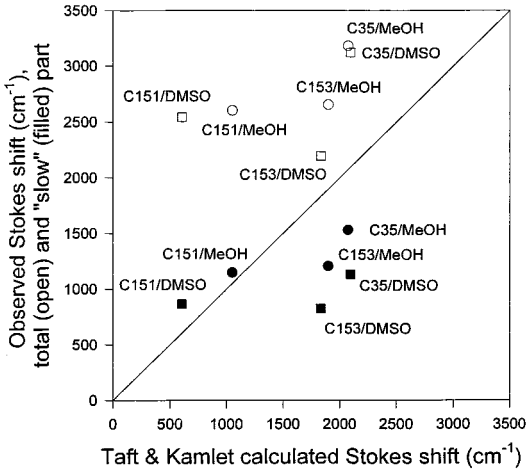

Figure 12. Correlation between observed dynamic Stokes shifts and the pure solvent contribution to the Stokes shift as calculated with the Kamlet and Taft model. Total observed Stokes shifts (including the ultrafast 50 fs component) are indicated by open symbols (MeOH, circles; DMSO, squares), while filled symbols correspond to only the slow part of the time-dependent shift (excluding the ultrafast 50 fs component).

It is tempting to apply this reasoning to the present case and compare the hydrogen bondings in methanol and DMSO once more for the three coumarins. Breaking (dissipating) occurs on the various sites of the amino group and forming (creating) occurs on the carbonyl site. Why does this not show up in the dynamics, as predicted by Phelps et al.?

Actually it does, the breakings of type A and type C hydrogen bonds are very fast and are mingled within our time resolution with the ultrafast component of the nonspecific solvation. This is the case for all three coumarins in both solvents. The forming of the type B hydrogen bond only occurs in methanol and is manifested by the slow 10−20 ps component (τ_3). In DMSO, the slow 15−30 ps component (τ_3) has a negligible preexponential factor (0.03−0.06), as can be seen in Table 6. We will now consider the discrepancies between the "slow" part of the Stokes shift and our "Kamlet and Taft" analysis. These discrepancies correspond to "missed" ultrafast solvent relaxation. Reexamining Figure 12 one can make three observations: (1) C151 in MeOH and DMSO fall on the line, (2) C35 and C153 fall 700 cm^{-1} from the line in MeOH, (3) C35 and C153 fall 1000 cm^{-1} from the line in DMSO.

We can make the following hypotheses: (A) For C151 in MeOH and DMSO the ultrafast inertial nonspecific polar solvation is exactly canceled by the breaking of the C type hydrogen bonds and there is no net ultrafast component of the solvation. The observed slow relaxation is well accounted for by the "Kamlet and Taft" analysis. (B) For C35 and C153 in MeOH, only the breaking of the type A hydrogen bond on the nitrogen lone pair compensates partly but not totally for the ultrafast inertial nonspecific polar solvation. This implies that the solvation energy calculated using the "Kamlet and Taft" model contains a large ultrafast contribution of roughly 700 cm^{-1}. (C) For C35 and C153 in DMSO there are no hydrogen bonds, so there is no canceling effect at all. All of the inertial component in the nonspecific polar solvation is present in the ultrafast relaxation. The slow solvent relaxation has an amplitude smaller by 1000 cm^{-1} than the solvation energy predicted by the "Kamlet and Taft" model.

We thus propose that the specific hydrogen bonding character of both the solute and the solvent has a large influence on the observed dynamics. Of course, this conjecture is of highly

TABLE 7: Literature Data on TDFSS Measurements in Methanol and DMSO Using Various Fluorescent Solutes[a]

TDFSS Measurements in Methanol

solute	RES (fs)	INT (ps)	model	A_1	τ_1	ω	A_2	τ_2	A_3	τ_3	A_4	τ_4	$\langle\tau\rangle$	$\tau_{1/e}$
C152[10]	≤100	50	2E				0.40	1.16			0.60	9.57	6.21	
C343[14]	150		2E				0.21	1.0			0.79	10.3	8.3	
C153[15]	75	1	2E	0.57	0.075		0.43	0.58						
C153[18]	75*	200	1G2E	0.22		12.8	0.23	0.56			0.34	8.1		
C153[21]	30	1100	4E	0.101	0.030		0.340	0.28	0.298	3.20	0.261	15.3	5.0	2.3
C102[23]	135*	15	3E	0.29	0.18				0.31	1.96	0.40	15.36	6.80	
DCM[39,41]	200*	30	2E	0.36	0.175				0.64	3.2			2.1	
LDS750[63]	350	200	1E							3.3			3.3	
DCM[64]	150	20	2E				0.75	0.5	0.25	4.3			1.5	
DASPI[65]	100	30	1G2E	0.14		6.0	0.75	1.3			0.11	12.4		1.0
DCM[66]	100	30	1G2E	0.20		6.0	0.50	0.7	0.3	5.0				1.0

TDFSS Measurements in DMSO

solute	RES	INT	model	A_1	τ_1	A_2	τ_2	A_3	τ_3	$\langle\tau\rangle$	$\tau_{1/e}$
C152[11]	130*	8	2E	0.57	0.33	0.43	2.3			1.2	
C153[13]	130**	30	2E	0.44	0.33	0.56	2.2			1.4	
C153[21]	30	1100	3E	0.500	0.214	0.408	2.29	0.092	10.7	2.0	0.90
LDS750[63]	350	200	1E				3.1			3.1	

[a] The RES column is the experimental time resolution (when it is not estimated by the authors, we give the exciting laser pulse width (denoted by **) or the instrument response function divided by 1.55 (denoted by *) (supposing a sech^2 pulse shape)). The INT column is the time interval in which the $c(t)$ function has been defined, most of these values are uncertain. The model column gives the character and the number of terms used in the model function used to fit $c(t)$, G = Gaussian, E = exponential. All times are given in picoseconds. In the case a Gaussian term was used, its value is given in $(\mathrm{ps})^{-1}$ and replaces τ_1.

speculative character, but it is interesting to use the information contained in the KT analysis of the steady-state absorption and fluorescence spectra, and which clearly demonstrates the importance of solute−solvent hydrogen bonding to gain more insight into the time evolution of the fluorescence spectra as well. Although we will have more to say about a comparison between theory and experiment in the next section, it is good to remark already at this point that, in recent theoretical work on solvation dynamics, where the complex molecular charge distribution of the solute is explicitly taken into account, it has been proposed that the magnitude of the inertial component is affected by "interference" between the solvation of different atomic sites in the molecule.[16,18,72] Our suggestions are, in fact, very much along these lines.

V. Discussion

We have thus shown that there is a correlation between the amplitude of the slow part of the experimentally observed Stokes shift and the solvent contribution to the total Stokes shift as calculated by the empirical method of Kamlet and Taft. However, this slow contribution alone is slightly less (C35 and C153) than or equal (C151) to estimations based on the Kamlet and Taft solute−solvent interaction model. This implies that part of the predicted solvent Stokes shift is not accounted for by the observed slow part, but might be embedded in the ultrafast component. The solvent induced Stokes shift given by the calculus is however much less than the time-resolved total spectral shift. This observation leads to the conclusion that the ultrafast component of the dynamic Stokes shift is mainly due to intramolecular relaxation. We will now discuss this in the light of other data published in the literature on solvation dynamics studies in methanol and DMSO.

Indeed, during the past few years a large number of experimental studies of solvation dynamics in methanol and DMSO have been reported in the literature. We will, however, restrict ourselves to recent femtosecond studies in methanol,[10,14,15,18,21,39,63−66] and DMSO.[5,8,11,13,21] Relevant data are regrouped in Table 7.

Inspecting these tables, some general remarks can be made. If all previous solvation dynamics studies (with the exception of ref 63) report nonexponential behavior and the presence of an ultrafast component, only a very recent work on methanol indicates that this component is unresolvably fast (<100 fs).[67] In DMSO, a large portion of the Stokes shift is sub-picosecond, but slow enough (200−300 fs) to be well characterized experimentally. Interestingly, the mean solvation times in methanol of coumarins (C152, C153, C343, and C102) are slower than those of other probe molecules (DCM and LDS750). This clearly demonstrates the influence of the probe molecule on the solvation dynamics.

All our measurements display an ultrarapid unresolved component in both methanol and DMSO. As just mentioned, this is not the first time such a fast component is reported for solvation dynamics in methanol, but its amplitude in our measurements is slightly larger than previously reported. In DMSO, the occurrence of an ultrafast (<100 fs) component is reported for the first time. Before going into details, one may argue that this is the result of the different experimental techniques and analysis methods used (see sections II.B, II.C, and IV.B). Although we have full confidence in our methods, we judge that it is important to obtain more information on this point.

Maroncelli and co-workers have provided the most detailed study of solvation dynamics to date.[21,22] They studied TDFSS in more than 30 polar and nonpolar, protic and aprotic solvents using the coumarin C153. In methanol and DMSO they found a highly nonexponential behavior of the correlation function $c(t)$, and in order to get good descriptions, they used four exponentials in the case of methanol and three exponentials for DMSO. The corresponding values are given in Table 7. With an experimental response function of about 100 fs and using the spectral reconstruction method[4] combined with an independent way to determine the time-zero spectra,[17] they claimed to observe all of the spectral evolution (both the inertial and the diffusive parts of the relaxation). In methanol they had to limit the ultrafast component to 30 fs (we did likewise, limiting the fastest component to 50 fs). The slower components observed

by them compare very well to our values, even though they used one additional exponential term. In particular, their average solvation time of 5.0 ps is identical to our value of 4.8 ps within the experimental and treatment error bars. More precisely, our 1/*e* time, 1.1 ps, shorter than their 2.3 ps, may be explained by the larger amplitude (55%) of our 50 fs component as compared to the 10% of their 30 fs component. But when taken into account, the two sub-picosecond components in their analysis (30 and 280 fs) represent 44% of the total shift. In DMSO, there is a relatively good agreement between our values and Maroncelli's, especially for what concerns the average solvation time, 1.7 ps (our value) vs 2.0 ps (their value). Once again, our measured 1/*e* time, 0.18 ps, is much shorter than their value of 0.90 ps, and the origin for this discrepancy can once again be ascribed to the large amplitude of the ultrafast (50 fs) component in our data. As mentioned above, the presence of such an ultrafast component in the case of DMSO was not observed by Maroncelli and co-workers, and this is an important qualitative and quantitative difference, which needs some comment.

Let us first note that Maroncelli discussed the possibility of intramolecular vibrational relaxation contributing to the observed Stokes shifts. However, by studying C153 in *n*-hexane, he noted the nearly total lack of temporal evolution of the fluorescence spectrum. This was found to be very much in contrast with the very dramatic changes predicted by the theory.[45] He concluded that intramolecular vibrational relaxation was unimportant compared to the solvent-induced spectral shifts.

If we compare our measured full rMDFSSs with the values given by Maroncelli they compare surprisingly well. However, for reasons given above to describe the pure solvent effect we prefer to use only the "slow" part of the time-resolved measurements which gives much smaller TDFSSs than Maroncelli's data. We thus believe that Maroncelli's TDFSSs contain also substantial contributions from intramolecular relaxation.

It is also interesting to compare our results with those from molecular dynamics (MD) studies on methanol.[16,18,60−62,68−72]. Unfortunately, there are no MD studies on DMSO. Before discussing the MD calculations on methanol solvation in detail, it is worthwhile to note that, prior to the methanol calculations, other MD simulations had been carried out in a simple aprotic model solvent,[73] acetonitrile,[74] and also in water.[75,76] These calculations predicted the existence of an important ultrafast component (about 100−250 fs in aprotics, 30 fs in water). In the literature it has become commonplace to designate this ultrafast component as being "inertial". The term inertial is thus used to describe both the ca. 100 fs component found in, for example, acetonitrile, which can be associated with small-angle rotations of individual solvent molecules[74] and the ca. 30 fs component observed in protic solvents such as water and methanol, which is mainly of O−H librational character.[61,70] In certain simulations the inertial component was found to account for up to 80% of the total Stokes shift,[73,74] a fact corroborated by experimental ultrafast TDFSS studies.[18,19,24,25] It should be mentioned though that some recent MD calculations on solvation dynamics in water, which treat polarizable solutes,[77,78] lead to the conclusion that this feature seems to decrease the importance of the ultrafast solvent relaxation.

Concentrating on molecular dynamics studies in methanol, early studies showed that the amplitude of the ultrafast inertial component was much reduced as compared to acetonitrile or water.

Ando and Kato studied the ionization of *N*,*N*-dimethylaniline (DMA) in water and methanol by molecular dynamics simulations.[68] In methanol, they observe a "slow" decay of 0.5−0.7 ps and less pronounced oscillations with a 60 fs period. The initial loss by the first oscillation is only 10−20%. The oscillatory motion is identified as solute−solvent interactions and assigned to the librational mode of solvent water molecules.

Fonseca and Ladanyi used a diatomic solute model in the MD simulations of solvation dynamics of an instantaneously created dipole in methanol.[61,70] They found that the linear response theory breaks down in this solvent (i.e., the energy fluctuation correlation functions of the nonpolar ground state and the dipolar excited state differed substantially). They found an initial Gaussian component, assigned to a free H-rotation around the Me-O bond. This ultrafast 30 fs component is somewhat hidden by librational motion, resulting from hydrogen bond restoring forces, a situation similar to what had been observed in water. Interestingly, the Gaussian term only accounts for 20% of the total response in the case of methanol.

Of more interest are the molecular dynamics studies explicitly treating the solvation of large solute molecules in methanol. Brown did MD simulations on 7-amino-3-methyl-1,4-benzoxazine-2-one in methanol,[71] the structure of which is fairly close to that of aminocoumarins. He did not give any detailed values for the solvation process except that, in the 0.5−5 ps interval, it is well described by a monoexponential with a 1.3 ps time constant. However, after inspection of his data, one can conclude to the presence of two ultrafast components, a Gaussian term (less than 20 fs time constant) and an oscillatory motion with a 50 fs period. The $c(t)$ function is down to 40% after 200 fs but the first oscillation accounts for less than 20%.

In early papers, Maroncelli and co-workers performed molecular dynamics simulations of coumarin C153 in methanol and compared the results with experimental data.[16,18] They found that the ultrafast (<100 fs) inertial component accounts for only 16% of the dynamics in the simulations, whereas their experimental data indicated an unresolvably fast component of about 50%. However, in a more recent paper, Kumar and Maroncelli, improving the molecular dynamics calculations and at the same time refining the experimental techniques and the analysis of data,[72] obtained a quite drastically changed picture. Their new MD results indicate the presence of two ultrafast Gaussian components, one with the frequency $\omega_s = 28$ ps^{-1} and a very high amplitude, 44%, but modulated by a second slower one. The resulting envelope may be fitted by a single Gaussian which is then slower and has a lower relative amplitude than the figures quoted above, but still is much faster and of higher amplitude than what was found by experiment. In fact, admitting that the capability of the simulations to reproduce the experimental observations is less satisfactory than expected, they conclude that the "inadequate representation of the dielectric properties of methanol" cause the disagreement (i.e., that the simulation dynamics are too fast).

To conclude this overview of literature MD simulations in methanol, it seems that the ultrafast sub-100 fs inertial component exists but only accounts for 10−20% of the total relaxation. This is in agreement with our conclusions from the comparison between steady-state and time-resolved data in the sense that the main part of the ultrafast time-resolved relaxation is of an intramolecular origin.

There are some additional reports in the literature that the solvent contribution to observed spectral shifts of coumarins in polar solution is fairly moderate. In their study of the photoinduced intermolecular electron-transfer reaction of the coumarin C337 in dimethylaniline (DMA), Walker and co-workers also performed a solvatochromic analysis of steady-

state fluorescence spectra.[79] They estimated that the solvent contribution in DMA only amounts to about 300 cm^{-1} as compared to the intramolecular Stokes shift of about 1530 cm^{-1}.

Regarding the influence of hydrogen bonds in a picosecond study of various solutes in propanol,[20] Maroncelli observed that the solute particularities have little influence on the solvation dynamics. In particular, for solutes with two or more hydrogen bonding sites (which is the case for the three coumarins treated in the present work), practically no differences were observed. He concluded that hydrogen bonding contributes to the solvation on the same time scale as the bulk relaxation. That solvation and hydrogen bond formation response functions decay at similar rates in methanol was also remarked by Skaf and Ladanyi.[62]

Berg and co-workers have studied the hydrogen bonding dynamics with a 1 ps time resolution using resorufin as a probe molecule almost insensitive to the solvent polarity.[80,81] In ethanol at room-temperature they concluded that hydrogen bond dynamics involves a hydrogen bond lifetime of 120 ps. They proposed a two-step model, a very fast initial bond breaking followed by a further solvent reorganization on a longer time scale.

Rullière and co-workers discussed the multiexponential TDFSSs observed in alcohols and compared the experimental long time constants with estimations of single (solvent) molecule reorientation times.[82,83] These estimated "microscopic" relaxation times were calculated using the theory developed by Kivelson and co-workers for the "high k limit" relaxation close to the excited solute molecule.[84,85] Even if a comparison with dielectric continuum models are outside the scope of this paper, it is very interesting to note that the value Rullière et al. gave for the "microscopic" relaxation time in methanol, 14 ps, is very close to the long-time constants we have observed. Rullière et al. argued that the "microscopic" relaxation time, corresponding to the noncooperative single molecule reorientation time equals the hydrogen bond formation time, and that this specific solute−solvent interaction takes place only if the newly created solute−solvent forces after photoexcitation are strong enough to break the hydrogen bonded solvent network.

In section IV.C we formulated a hypothetical model based on a canceling effect between the ultrafast inertial solvent relaxation and the hydrogen bond breaking on the amino group. These two processes are supposedly much faster than our experimental time-resolution of 50 fs. The hydrogen bond formation on the carbonyl group, in the case of methanol, is supposedly much slower, between 10 and 20 ps. It would be interesting to compare these characteristic times for the solute−solvent interaction dynamics with the dynamics of neat methanol and to address the question of how the solvent−solvent interaction dynamics affect the specific solute−solvent interaction dynamics.

Data on pure methanol relaxation dynamics are available from, among others, Optical Kerr Effect (OKE) measurements,[86,87] dielectric relaxation measurements,[88,89] and molecular dynamics (MD) simulations.[90−93] From these investigations one may conclude that there is evidence that the hydrogen bonding properties of pure methanol makes it an intrinsically "slower" solvent than aprotic solvents such as DMSO. However, as calculated by MD, the typical hydrogen bond lifetime is on the order of 1−2 ps, which is much faster than the long relaxation time observed in our solvation experiment. Moreover, neat methanol dynamics, as observed in optically heterodyne detected optical kerr effect (OHD-OKE) measurements, is faster than the dynamics found in solvation experiments, in particular if the measured polarizability anisotropy correlation function is converted into a solvation correlation function.[94] Only dielectric relaxation data of methanol shows the presence of a slow relaxation time, but within the framework of the simple dielectric continuum theory[12] (e.g., $\tau_S \approx \tau_D(\epsilon_\infty/\epsilon_0)$ where τ_D is the measured dielectric relaxation time, ϵ_∞ is the dielectric constant in the high-frequency limit, and ϵ_0 the static dielectric constant) this dielectric relaxation time τ_D translates into a solvation time τ_S much less than 10 ps. The exact microscopic nature of this component is not exactly known, but it is commonly supposed that it is related to many-body cooperative, diffusional motion. We are thus led to conclude that the ca. 15 ps relaxation time observed in our solvation experiments has no direct analogue in neat methanol.

We have argued in the preceding section that the long-time constant (10−20 ps) observed in our solvation studies in the protic solvent methanol corresponds to the formation of a hydrogen bond on the carbonyl group. This was based on the results from a separate solvatochromic study. It now appears that additional support for this conjecture can be obtained from a comparison of the characteristic times observed in our solvation experiments with those measured in the neat liquid (see references in the preceding paragraph). Of course, the time scale for the solute−solvent H-bond formation may be strongly influenced by the solvent's cooperative diffusional dynamics as the local motion around the coumarin carbonyl site will probably involve a larger portion of the methanol H-bond network.

Conclusion

In the case of the presently studied aminocoumarins, the comparison of our time-resolved Stokes shifts and calculated values from the steady-state data using the Kamlet and Taft model shows that the observed dynamic Stokes shift cannot be accounted for only by the solvent contribution and that the main part must be due to intramolecular relaxation. We believe that after the initial hydrogen bond breaking and ultrafast inertial dipolar relaxation (<50 fs) observed in the HBA DMSO and HBD methanol, and after the diffusional solvent relaxation on the order of a few picoseconds, hydrogen bond formation at the carbonyl group occurs on the 10−20 ps time scale, as observed in the HBD methanol.

Acknowledgment. We gratefully acknowledge the interest of the Groupement de recherches 1017 of the CNRS.

Appendix

The definition of the mean frequency is

$$\bar{\nu}(t) = \frac{\int_{-\infty}^{\infty} I(\nu,t)\nu \, d\nu}{\int_{-\infty}^{\infty} I(\nu,t) \, d\nu} = \frac{\int_{-\infty}^{\infty} I(\nu,t)\nu \, d\nu}{I(t)} \qquad \text{(A1)}$$

where the denominator may be identified with the observed intensity $I(t)$, integrated over frequency, which of course is easily evaluated from experimental data. $I(\nu,t)$ is the experimentally recorded spectrum, constituting a surface (i.e., intensity vs frequency in wavenumbers and delay time). Actually, instead of the mean frequency, as defined by eq A1, we will focus on the time dependent Stokes shift of the mean frequency, defined as

$$\delta\bar{\nu}(t) = \bar{\nu}(t) - \bar{\nu}(\infty) \qquad \text{(A2)}$$

where $\bar{\nu}(\infty)$ is the mean frequency of the fully relaxed spectrum, which in all cases may be taken as the steady-state spectrum. It should be noted that $\bar{\nu}(\infty)$ is a constant. Using eqs. A1 and A2, one obtains easily

$$\delta\bar{\nu}(t) = \frac{\int_{-\infty}^{\infty} I(\nu,t)(\nu - \bar{\nu}(\infty))\,\mathrm{d}\nu}{\int_{-\infty}^{\infty} I(\nu,t)\,\mathrm{d}\nu} = \frac{\int_{-\infty}^{\infty} I(\nu,t)(\nu - \bar{\nu}(\infty))\,\mathrm{d}\nu}{I(t)} \tag{A3}$$

Although time-resolved fluorescence is a four-wave mixing process,[95] under our experimental conditions we assume that the effect of nonlinear terms can be neglected. Consequently, we can describe the experimental surface $I(\nu,t)$ with the convolution between a hypothetical model surface $\Phi(\nu,t)$ and the temporal response function $R(t)$. In doing so, we neglect the frequency dependence of the response function. For practical reasons we write the integral limits between plus and minus infinity; the causality principle is, however, not violated since the model function $\Phi(\nu,t)$ is uniformly zero for negative times.

$$I(\nu,t) = \int_{-\infty}^{\infty} R(t' - t)\Phi(\nu,t)\,\mathrm{d}t' \tag{A4}$$

We can now develop the expressions for the nominator and the denominator in eq A3 by inserting $I(\nu,t)$ according to eq A4. Starting with the nominator we have

$$\delta\bar{\nu}(t)I(t) = \int_{-\infty}^{\infty} I(\nu,t)(\nu - \bar{\nu}(\infty))\,\mathrm{d}\nu = \int_{-\infty}^{\infty}\int_{-\infty}^{\infty} R(t' - t)\Phi(\nu,t)\,\mathrm{d}t'(\nu - \bar{\nu}(\infty))\,\mathrm{d}\nu = \int_{-\infty}^{\infty}\left[\int_{-\infty}^{\infty}\Phi(\nu,t)(\nu - \bar{\nu}(\infty))\,\mathrm{d}\nu\right]R(t' - t)\,\mathrm{d}t' = \int_{-\infty}^{\infty} f(t)R(t' - t)\,\mathrm{d}t' \tag{A5}$$

Second, we do the same thing with the denominator, which is the integrated observed intensity.

$$\int_{-\infty}^{\infty} I(\nu,t)\,\mathrm{d}\nu = \int_{-\infty}^{\infty}\int_{-\infty}^{\infty} R(t' - t)\Phi(\nu,t)\,\mathrm{d}t'\,\mathrm{d}\nu = \int_{-\infty}^{\infty}\left[\int_{-\infty}^{\infty}\Phi(\nu,t)\,\mathrm{d}\nu\right]R(t' - t)\,\mathrm{d}t' = \int_{-\infty}^{\infty} i(t)R(t' - t)\,\mathrm{d}t' \tag{A6}$$

It should be emphasized that we do not explicitly consider the shape and the time evolution of the whole surface $\Phi(\nu,t)$, we only assume that the time evolution of the two integrals ($i(t)$ and $f(t)$) can be modeled analytically. The "real" mean frequency dynamic Stokes shift (rMFDSS) may be defined in analogy with eq A3 as

$$\Delta\bar{\nu}(t) = \bar{\nu}'(t) - \bar{\nu}'(\infty) = \frac{\int_{-\infty}^{\infty}\Phi(\nu,t)(\nu - \bar{\nu}(\infty))\,\mathrm{d}\nu}{\int_{-\infty}^{\infty}\Phi(\nu,t)\,\mathrm{d}\nu} \tag{A7}$$

where the primes indicate that the integral is over $\Phi(\nu,t)$, not $I(\nu,t)$. The interesting point in eq A7 is that the nominator and the denominator are exactly the functions $f(t)$ and $i(t)$ defined previously in eqs A5 and A6. Using a trick and writing $f(t) = g(t)i(t)$ ($t>0$) we can thus simply write

$$\Delta\bar{\nu}(t) = \frac{f(t)}{i(t)} = \frac{g(t)i(t)}{i(t)} = g(t) \tag{A8}$$

where $g(t)$ corresponds to the "true" spectral shift and $i(t)$ to the "true" integrated intensity of the nonconvoluted surface $\Phi(\nu,t)$.

For the model functions we choose ($t>0$):

$$f(t) = g(t)i(t) = \int_{-\infty}^{\infty}\Phi(t)(\nu - \bar{\nu}(\infty))\,\mathrm{d}\nu = \Delta\bar{\nu}[\alpha\mathrm{e}^{-t/\tau_1} + \beta\mathrm{e}^{-t/\tau_2} + \gamma\mathrm{e}^{-t/\tau_3}]i(t) \tag{A9}$$

with $\alpha + \beta + \gamma = 1$ and

$$i(t) = \int_{-\infty}^{\infty}\Phi(t)\,\mathrm{d}\nu = I_0[1 + \varphi\mathrm{e}^{-t/\tau_3} - \theta\mathrm{e}^{-t/\tau_4}] \tag{A10}$$

The observables used in the fitting process are the time-dependent fluorescence Stokes shift $\delta\bar{\nu}(t) = \bar{\nu}(t) - \bar{\nu}(\infty)$ and the integrated fluorescence intensity $I(t)$. The product $\delta\bar{\nu}(t)I(t)$ is calculated and together with the integrated intensity $I(t)$ these two are fitted/convoluted simultaneously using the procedure and the model functions described above.

References and Notes

(1) Jones, G., II In *Dye Laser Principles with Applications*; Duarte, F. J., Hillman, L. W., Eds. Academic Press: New York, 1990; pp 287−343.

(2) Drexhage, K. H. In *Dye Lasers*; Schafer, F. P., Ed.; Springer-Verlag: Berlin, 1993; pp 155−200.

(3) Lopez Arbeloa, T.; Lopez Arbeloa, F.; Tapia, M. J.; Lopez Arbeloa, I. *J. Phys. Chem.* **1993**, *97*, 4704.

(4) Maroncelli, M.; Fleming, G. R. *J. Chem. Phys.* **1987**, *86*, 6221.

(5) Kahlow, M. A.; Kang, T. J.; Barbara, P. F. *J. Phys. Chem.* **1987**, *91*, 6452.

(6) Castner, E. W.; Bagchi, B.; Maroncelli, M.; Webb, S. P.; Ruggiero, A. J.; Fleming, G. R. *Ber. Bunsen-Ges. Phys. Chem.* **1988**, *92*, 363.

(7) Maroncelli, M.; Fleming, G. R. *J. Chem. Phys.* **1988**, *89*, 875.

(8) Kahlow, M. A.; Kang, T. J.; Barbara, P. F. *J. Chem. Phys.* **1988**, *88*, 2372.

(9) Jarzeba, W.; Walker, G. C.; Johnson, A. E.; Kahlow, M. A.; Barbara, P. F. *J. Phys. Chem.* **1988**, *92*, 7039.

(10) Kahlow, M. A.; Jarzeba, W.; Kang, T. J.; Barbara, P. F. *J. Chem. Phys.* **1989**, *90*, 151.

(11) Walker, G. C.; Jarzeba, W.; Kang, T. J.; Johnson, A. E.; Barbara, P. F. *J. Opt. Soc. Am. B* **1990**, *7*, 1521.

(12) Barbara, P. F.; Jarzeba, W. *Adv. Photochem.* **1990**, *15*, 1.

(13) Jarzeba, W.; Walker, G. C.; Johnson, A. E.; Barbara, P. F. *Chem. Phys.* **1991**, *152*, 57.

(14) Johnson, A. E.; Tominaga, K.; Walker, G. C.; Jarzeba, W.; Barbara, P. F. *Pure Appl. Chem.* **1993**, *65*, 1677.

(15) Rosenthal, S. J.; Scherer, N. F.; Cho, M.; Xie, X.; Schmidt, M. E.; Fleming, G. R. In *Ultrafast Phenomena VIII*, Martin, J.-L., Migus, A., Mourou, G. A., Zewail, A. H., Eds.; Springer-Verlag: Berlin, 1993; pp 616−617.

(16) Maroncelli, M.; Kumar, P. V.; Papazyan, A.; Horng, M. L.; Rosenthal, S. J.; Fleming, G. R. In *Ultrafast Reaction Dynamics and Solvent Effects*; Rossky, P., Gauduel, Y., Eds.; American Institute of Physics Press: New York, 1994; pp 310−333.

(17) Fee, R. S.; Maroncelli, M. *Chem. Phys.* **1994**, *183*, 235.

(18) Rosenthal, S. J.; Jimenez, R.; Fleming, G. R.; Kumar, P. V.; Maroncelli, M. *J. Mol. Liq.* **1994**, *60*, 25.

(19) Jimenez, R.; Fleming, G. R.; Kumar, P. V.; Maroncelli, M. *Nature* **1994**, *369*, 471.

(20) Chapman, C. F.; Fee, R. S.; Maroncelli, M. *J. Phys. Chem.* **1995**, *99*, 4811.

(21) Horng, M. L.; Gardecki, J. A.; Papazyan, A.; Maroncelli, M. *J. Phys. Chem.* **1995**, *99*, 17311.

(22) Reynolds, L.; Gardecki, J. A.; Frankland, S. J. V.; Horng, M. L.; Maroncelli, M. *J. Phys. Chem.* **1996**, *100*, 10337.

(23) Shirota, H.; Pal, H.; Tominaga, K.; Yoshihara, K. *J. Phys. Chem.* **1996**, *100*, 14575.

(24) Rosenthal, S. J.; Xie, X.; Du, M.; Fleming, G. R. *J. Chem. Phys.* **1991**, 95, 4715.

(25) Cho, M.; Rosenthal, S. J.; Scherer, N. F.; Ziegler, L. D.; Fleming, G. R. *J. Chem. Phys.* **1992**, *96*, 5033.
(26) Rettig, W.; Klock, A. *Can. J. Chem.* **1984**, *63*, 1649.
(27) Masilamani, V.; Chandrasekar, V.; Sivaram, B. M.; Sivasankar, B.; Natarajan, S. *Opt. Commun.* **1986**, 59, 203.
(28) Jones, G., II; Jackson, W. R.; Choi, C.; Bergmark, W. R. *J. Phys. Chem.* **1985**, *89*, 294.
(29) Jones II, G.; Jackson, W. R.; Kanoktanaporn, S.; Halpern, A. M. *Opt. Commun.* **1980**, *33*, 315.
(30) Chu, G.; Yangbo, F. *J. Chem. Soc., Faraday Trans.* **1987**, *83*, 2533.
(31) Rechthaler, K.; Köhler, G. *Chem. Phys.* **1994**, *189*, 99.
(32) Kovalenko, S. A.; Ruthmann, J.; Ernsting, N. P. *Chem. Phys. Lett.* **1997**, *271*, 40.
(33) McCarthy, P. K.; Blanchard, G. J. *J. Phys. Chem.* **1993**, *97*, 12205.
(34) Jiang, Y.; McCarthy, P. K.; Blanchard, G. J. *Chem. Phys.* **1994**, *183*, 249.
(35) Köhler, G.; Rechthaler, K. *Pure Appl. Chem.* **1993**, *65*, 1647.
(36) Shah, J. *IEEE J. Quantum Electron.* **1988**, *24*, 276.
(37) Kahlow, M. A.; Jarzeba, W.; DuBruil, T. P.; Barbara, P. F. *Rev. Sci. Instrum.* **1988**, *59*, 1098.
(38) Mokhtari, A.; Chebira, A.; Chesnoy, J. *J. Opt. Soc. Am. B* **1990**, *7*, 1551.
(39) Gustavsson, T.; Baldacchino, G.; Mialocq, J.-C.; Pommeret, S. *Chem. Phys. Lett.* **1995**, *236*, 587.
(40) Johnson, F. M. In *Handbook of Lasers*; CRC Press: Cleveland, OH, 1971; p 526.
(41) Pommeret, S.; Gustavsson, T.; Naskrecki, R.; Baldacchino, G.; Mialocq, J.-C. *J. Mol. Liq.* **1995**, *64*, 101.
(42) Siano, D. B.; Metzler, D. E. *J. Chem. Phys.* **1969**, *51*, 1856.
(43) The ratio between our and Maroncelli's Stokes shifts values is almost constant for all solvents, increasing from 1.10 in *n*-hexane to 1.12 in methanol.
(44) Our measured fwhm values for the absorption spectra of C153 increases more with the observed Stokes than what was reported by Maroncelli and co-workers.[21] They gave, however, values obtained from $p(\delta)$ distribution function. Our measured fwhm values for the emission spectra of C153 remain constant, similar to Maroncelli's data.
(45) See refs 106−107 of ref 21.
(46) Lippert, E. *Z. Naturforsch.* **1855**, *10A*, 541.
(47) Dimroth, K.; Reichardt, C.; Siepmann, T.; Bohlmann, F. *Liebigs Ann. Chem.* **1963**, *661*, 1.
(48) Reichardt, C. *Chem. Rev.* **1994**, *94*, 2319.
(49) Kamlet, M. J.; Abboud, J. L.; Taft, R. W. *J. Am. Chem. Soc.* **1977**, *99*, 6027.
(50) Kamlet, M. J.; Dickinson, C.; Taft, R. W.; *Chem. Phys. Lett.* **1981**, 77, 69.
(51) Kamlet, M. J.; Abboud, J. L. M.; Abraham, M. H.; Taft, R. W. *J. Org. Chem.* **1983**, *48*, 2877
(52) Marcus, Y.; Kamlet, M. J.; Taft, R. W. *J. Phys. Chem.* **1988**, *92*, 3613.
(53) Riddick, J. A.; Bunger, W. B.; Sakano, T. K. *Organic Solvents. Physical Properties and Methods of Purification*; John Wiley & Sons: New York, 1986.
(54) Brooker, L. G. S. *J. Am. Chem. Soc.* **1965**, *87*, 2443.
(55) Cassara, L.; Gustavsson, T.; Pommeret, S.; van der Meulen, P.; Mialocq, J.-C. Unpublished data.
(56) Actually, is is important to note that the stability of the solution was checked by comparing steady-state spectra recorded before and after the upconversion experiment.
(57) With deconvolution we understand the numerical procedure consisting of the convolution and iterative nonlinear fitting of a model function to experimental data.
(58) With "real" mean frequency we understand the mean frequency of the nonconvoluted intensity surface which can be approximated with the model function intensity surface, see Appendix I.
(59) Note that these quantities refer to the model functions introduced in Appendix I. It can equally well be written in the usual manner $c(t) = (\bar{\nu}(t) - \bar{\nu}(\infty))/(\bar{\nu}(0) - \bar{\nu}(\infty))$ but we prefer not taking the risk to confuse raw data and model functions (i.e., the mean frequency can be defined as well from raw data as from the model functions).
(60) Phelps, D. K.; Weaver, M. J.; Ladanyi, B. M. *Chem. Phys.* **1993**, *176*, 575.
(61) Fonseca, T.; Ladanyi, B. M. *J. Phys. Chem.* **1991**, *95*, 2116.
(62) Skaf, M. S.; Ladanyi B. M. *J. Phys. Chem.* **1996**, *100*, 18258.
(63) Castner, E. W.; Maroncelli, M.; Fleming, G. R. *J. Chem. Phys.* **1987**, *86*, 1090.
(64) Zhang, H.; Jonkman, A. M.; van der Meulen, P. Glasbeek, M. *Chem. Phys. Lett.* **1994**, *224*, 551.
(65) Jonkman, A. M.; van der Meulen, P.; Zhang, H.; Glasbeek, M. *Chem. Phys. Lett.* **1996**, *256*, 21.
(66) Van der Meulen, P.; Zhang, H.; Jonkman, A. M.; Glasbeek, M. *J. Phys. Chem.* **1996**, *100*, 5367.
(67) Inspired by the results from molecular dynamics simulations, showing the presence of an initial ultrafast Gaussian component of inertial origin, experimental data were analyzed using such a Gaussian term during some time. It is now more or less accepted that, in the case of methanol at least, this component is too fast to resolve with today's experimental equipment (see ref 72).
(68) Ando, K.; Kato, S. *J. Chem. Phys.* **1991**, *95*, 5966.
(69) Zhu, J.; Cukier, R. I. *J. Chem. Phys.* **1993**, *98*, 5679.
(70) Fonseca, T.; Ladanyi, B. M. *J. Mol. Liq.* **1994**, *60*, 1.
(71) Brown, R. *J. Chem. Phys.* **1995**, *102*, 9069.
(72) Kumar, P. V.; Maroncelli, M. *J. Chem. Phys.* **1995**, *103*, 3038.
(73) Carter, E. A.; Hynes, J. T. *J. Chem. Phys.* **1991**, *94*, 5961.
(74) Maroncelli, M. *J. Chem. Phys.* **1991**, *94*, 2084.
(75) Maroncelli, M.; Fleming, G. R. *J. Chem. Phys.* **1988**, *89*, 5044.
(76) Bader, J. S.; Chandler, D. *Chem. Phys. Lett.* **1989**, *157*, 501.
(77) Bursulaya, B. D.; Zichi, D. A.; Kim, H. J. *J. Phys. Chem.* **1995**, *99*, 10069.
(78) Bursulaya, B. D.; Zichi, D. A.; Kim, H. J. *J. Phys. Chem.* **1996**, *100*, 1392.
(79) Wang, C.; Akhremitchev, B.; Walker, G. C. *J. Phys. Chem.* **1997**, *101*, 2735.
(80) Yu, J.; Berg, M. *Chem. Phys. Lett.* **1993**, *208*, 315.
(81) Benigno, A. J.; Ahmed, E.; Berg, M. *J. Chem. Phys.* **1996**, *104*, 7382.
(82) Declémy, A.; Rullière, C. In *Ultrafast Reaction Dynamics and Solvent Effects*; Rossky, P., Gauduel, Y., Eds.; American Institute of Physics Press: New York, 1994; pp 275−295.
(83) Declémy, A.; Rullière, C.; Kottis, P. *Laser Chem.* **1990**, *10*, 413.
(84) Madden, P.; Kivelson, D. *Adv. Chem. Phys.* **1984**, *56*, 467.
(85) Friedrich, V.; Kivelson, D. *J. Chem. Phys.* **1987**, *86*, 6425.
(86) Cho, M.; Du, M.; Scherer, N. F.; Fleming, G. R. *J. Chem. Phys.* **1993**, *99*, 2410.
(87) Shirota, H.; Yoshihara, K.; Smith, N. A.; Lin, S.; Meech, S. R. *Chem. Phys. Lett.* **1997**, *281*, 27.
(88) Barthel, J.; Bachhuber, K.; Buchner, R.; Hetzenauer, H., *Chem. Phys. Lett.* **1990**, *165*, 369.
(89) Kindt, J. T.; Schmuttenmaer, C. A. *J. Phys. Chem.* **1996**, *100*, 10373.
(90) Haughney, M.; Ferrario, M.; McDonald, I. R. *J. Phys. Chem.* **1987**, *91*, 4934.
(91) Ferrario, M.; Haughney, M.; McDonald, I. R.; Klein, M. L. *J. Phys. Chem.* **1990**, *93*, 5156.
(92) Alonso, J.; Bermejo, F. J.; Garcia-Hernandez, M.; Martinez, J. L.; Howells, W. S. *J. Mol. Struct.* **1991**, *250*, 147.
(93) Ladanyi, B. M.; Liang, Y. Q. *J. Chem. Phys.* **1995**, *103*, 6325.
(94) Chang, Y. J.; Castner, Jr. E. W. *J. Phys. Chem.* **1996**, *100*, 3330.
(95) Mukamel, S. *Principles of Nonlinear Spectroscopy*; Oxford University Press: Oxford, 1995.